№1, 2022 ISSN 2706-977X

MATERIAL AND MECHANICAL ENGINEERING TECHNOLOGY

Material and Mechanical Engineering Technology | MMET.KZ

Content

DOI 10.52209/2706-977X_2022_3 IRSTI 55.03.14 UDC 621.313.13(045)

Development of an Inductor for the "Stator" Part

Malashkevichute – Brillant E.I., Medvedeva I.E.*, Tulegenova Sh.N.
Karaganda Technical University, Karaganda, Kazakhstan
*corresponding author

Abstract: To simplify and facilitate the process of high-frequency hardening of the “stator” part, an inductor with sprayer cooling was developed, which has a sectional design. In this case, a frequency of 50 Hz is suitable for the inductor. In this case, the generator voltage will be 750 V. The heating time for a part with such a diameter, at such a frequency, will be about 120 seconds. During spray hardening, the wall thickness of the active part of the inductor is taken equal to 4 ... 6 mm; the inductor in this case is made cast or welded from separate sheets. To avoid closing the turns of the inductor, they are isolated with an asbestos cord impregnated with liquid glass. The design feature is that the workpiece placed in the inductor is, as it were, a single-turn secondary coil of a high-frequency transformer, therefore the current arising in it has a direction opposite to the current flowing in the inductor.

Keywords: Heat treatment, coupling, induction heating, inductor, steel, stator.

Introduction

A stator (coupling) is a device used to connect shaft ends, rods, pipes, electrical wires, etc. The need for shaft connections is due to the fact that most machines are assembled from a number of separate parts with input and output shafts, which are connected using couplings. Shaft coupling is a general purpose, but not the only one. For example, clutches are used to turn the actuator on and off while the engine is running continuously (controlled clutches); protection of the machine from overload (safety clutches); compensation for the harmful effects of shaft misalignment (compensating couplings); reduction of dynamic loads (elastic couplings), etc. [1]. The toothed coupling compensates for all types of shaft misalignment. Shaft misalignment compensation during clutch operation is accompanied by a torque, bending moment, shearing (radial) and axial force. The main areas of application are long shaft lines, as well as shafts with limited dimensions. The stator is operated under difficult stressful conditions and experiences high dynamic loads. The material must have a high surface hardness combined with a soft core. Steel 40X possesses such properties. After improvement and surface hardening with HFC heating, parts from this steel grade meet the requirements of high surface hardness and increased wear resistance. The initial heat treatment of the 40X steel pin is annealing. Annealing simultaneously provides a fine-grained structure and an improvement in the structure of the steel to facilitate subsequent machining. [2]

Induction heating of the metal occurs in an inductor, which is one of the main elements of a high-frequency installation, which largely determines the efficiency of the installation and the shape of the hardened layer. The inductor is a coil made of round or rectangular copper tubes. It is necessary that the wall thickness of the tube is greater than the depth of current penetration into copper.

For an inductor cooled with water during the entire period of operation, the wall thickness is 1.5 ... 2 mm. During spray quenching, when water enters the tubes only at the moment of cooling, the thickness of the walls of the active part of the inductor is taken to be 4 ... 6 mm; the inductor in this case is made cast or welded from separate sheets

To avoid short-circuiting the turns of the inductor, they are insulated with an asbestos cord impregnated with liquid glass. [2].

When installing the part into the inductor, it is necessary to observe the uniformity of the gap A (Figure 1). It is not allowed to touch the part and the inductor during heating.

To increase the durability of the inductor and reduce heat loss by the heated workpiece, the inductor coil is covered with thermal insulation inside. A significant increase in the gap between the inner surface of the inductor and the workpiece leads to a decrease in efficiency. installation. Therefore, the thickness of the insulation layer is no more than 15 - 20 mm, and the inner diameter of the inductor coil is only 35 - 50 mm larger than the diameter of the workpiece. The length of the coil is taken 1 - 2 diameters longer than the length of the workpiece.

The workpiece, placed in the inductor, is, as it were, a single-turn secondary coil of a high-frequency transformer, therefore, the current arising in it has a direction opposite to the current flowing in the inductor. The current induced in the heated workpiece is unevenly distributed over the cross section. Figure 1 shows the location of the part in the inductor [3].

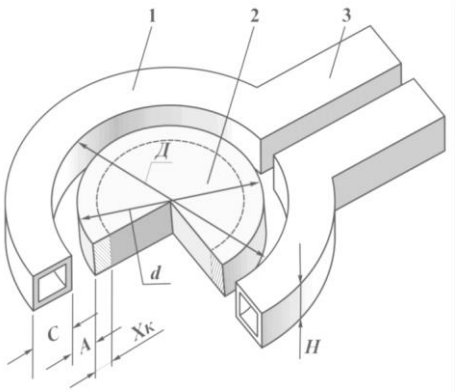

1 - inductor, 2 - part, 3 - bus; H is the height of the inductor, C is the width of the inductor, A is the air gap, Xk is the heated layer of the part [3]

Fig. 1. - System inductor - part

1. Methodology

To simplify and facilitate the process of hardening by high-frequency currents of the "stator" part, a spray-cooled inductor with a sectional design was developed (Figure 2).

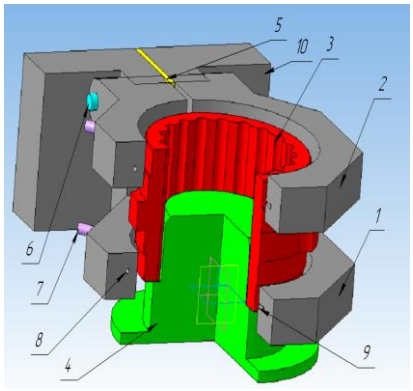

1 - lower part; 2 - upper movable part; 3 - heated workpiece; 4 - ceramic support; 5 - liquid glass gasket; 6 - ceramic rod; 7 - tube for supplying water to the inductor; 8 - hole for water circulation and inductor cooling; 9 - holes for water to exit to the surface to be hardened; 10 - block for supplying current

Fig. 2. - Sectional inductor for hardening the "stator" part

The principle of hardening is as follows: The purpose of the calculation is to determine the power of the inductor, the number of turns of the inductor and their cross section, as well as the strength of the current passing through the inductor1. Net power required to heat the workpiece to the final temperature.

The inductor is fixed by means of a movable carriage at a height of 40 mm from the surface of the working table of the unit. The upper part of the inductor 2 is movable, lifting it up, the workpiece 3 is installed on the ceramic support 4, after which the upper part is brought to its original position. Then the hoses of the pump pumping water for cooling the inductor and hardening the heated surface through the holes 7 and 9 are supplied to the pipes 7.

2. Results and discussion

1. Further, through the blocks 10, the workpiece is hardened and quenched, after the end of heating, the current supply is stopped and the water supply is turned on for quenching and cooling the inductor:

$$P_{\text{wor}} = \frac{g * c_{\text{м}} * (t_{\text{м}} - 20)}{0{,}24 * \tau}$$

where $t_{\text{м}}$- metal heating temperature, $t_{\text{м}}$=120^0C;

$c_{\text{м}}$ - average specific heat capacity of steel from 20 to 120^0C.

0.17 kcal/kg*deg

$$P_{\text{wor}} = \frac{12{,}3*0{,}17*(1200-20)}{0{,}24*120} = 87{,}125\text{kW}.$$

Electrical efficiency inductor is the ratio of the active resistance introduced by the workpiece to the total active resistance. Therefore, to determine it, it is necessary to know the active and reactance.

2. The active resistance of the inductor is determined by the formula:

$$R_1 = \rho_1 * \frac{\pi * d_{\text{ind}}}{l_{\text{ind}} \Delta_{\text{ind}}},$$

where ρ_1- electrical resistivity of copper at $40C$, equal $1{,}9 * 10^{-6}$ohm *cm;

Δ_{ind} - depth of current penetration into the material.

At a frequency of 50 Hz, the depth of current penetration into copper at $40°C$ is 10 mm.

$$R_1 = 1{,}9 * 10^{-6} * \frac{3{,}14*25}{4*1} = 37{,}28 * 10^{-6}\text{ohm}$$

3. The active resistance introduced by the heated workpiece is found by the formula:

$$R_2 = 6{,}2 * 10^{-8} * f * \frac{d_{\text{wor}^2}}{l_{\text{wor}}} * \text{A},$$

where f- current frequency equal to 50 Hz;

d_{wor} and l_{wor} - diameter and length of the hardened part, cm;

A is the function f(p), which characterizes the effect of the ratio of the workpiece diameter to the depth of current penetration into the heated steel on the value of the reduced active resistance of the workpiece, is found along the curves shown in figure 4.

$$p = \frac{\sqrt{2}}{2} * \frac{d_{\text{wor}}}{\Delta_{\text{wor}}},$$

where Δ_{wor}- the depth of penetration of current into the work piece for steel at a temperature of $760° C$.

The depth will be equal to 70 mm.

$$p = \frac{\sqrt{2}}{2} * \frac{200}{70} \approx 2$$

For the value p = 2, coefficient $A \approx 0{,}34$

This means that the active resistance introduced by the work piece will be equal to:

$$R_2 = 6{,}2 * 10^{-8} * 50 * \frac{20^2}{2{,}4} * 0{,}34 = 155 * 10^{-6}\text{ohm}.$$

4. Inductor reactance:

$$X_1 = 6{,}2 * 10^{-8} * f * \frac{d_{\text{ind}^2}}{l_{\text{ind}}} = 6{,}2 * 10^{-8} * 50 * \frac{25^2}{4} = 484{,}37 * 10^{-6}\text{ohm}.$$

5. The reactance introduced by the heated work piece:

$$X_2 = 6{,}2 * 10^{-8} * f * \frac{d_{\text{заг}^2}}{l_{\text{заг}}} * (1 - \text{B}),$$

Coefficient B is determined from Figure 23, depending on the parameter p. For the value p = 2, the coefficient B = 0.73.

$$X_2 = 6{,}2 * 10^{-8} * 50 * \frac{20^2}{4} * (1 - 0{,}73) = 361{,}66 * 10^{-6}\text{ohm}.$$

6. Equivalent active and reactance of the inductor, referred to one turn:

$$R_э = R_1 + R_2 = 155 * 10^{-6} + 37{,}28 * 10^{-6} = 192{,}28 * 10^{-6}\text{ohm}.$$

$$X_э = X_1 + X_2 = 484{,}37 * 10^{-6} + 361{,}66 * 10^{-6} = 846{,}03 * 10^{-6}\text{ohm}.$$

7. The total resistance of the inductor, referred to one turn:

$$z' = \sqrt{R_{э^2} + X_{э^2}} = \sqrt{(192{,}28 * 10^{-6})^2 + (846{,}03 * 10^{-6})^2} = 867{,}6 * 10^{-6}\text{ohm}.$$

8. Inductor power factor:

$$\cos\varphi = \frac{R_э}{z'} = \frac{192{,}28 * 10^{-6}}{867{,}6 * 10^{-6}} = 0{,}22$$

9. Electrical efficiency factor of inductor:

$$\eta_э = \frac{R_2}{R_э} = \frac{155 * 10^{-6}}{192{,}28 * 10^{-6}} = 0{,}8$$

10. Full efficiency factor:

$$\eta = \eta_э * \eta_t = 0{,}8 * 0{,}9 = 0{,}72$$

11. Power supplied to the inductor:

$$P_u = \frac{P_н}{\eta} = \frac{87{,}125}{0{,}72} = 121\text{kW}$$

12. Number of turns of the inductor:

$$\omega = \frac{u}{z'} * \sqrt{\frac{R_э * 10^{-3}}{P_u}}$$

where u - the voltage on the inductor supplied by the generator, usually equal to 750 V.

$$\omega = \frac{u}{z'} * \sqrt{\frac{R_э * 10^{-3}}{P_u}} = \frac{750}{867{,}6 * 10^{-6}} * \sqrt{\frac{192{,}28 * 10^{-6} * 10^{-3}}{121}} = 34 \text{ turn.}$$

13. Inductor current:

$$I_u = \frac{u}{\varpi^2 * z'} = \frac{750}{34^2 * 867{,}6 * 10^{-6}} = 747\text{A.}$$

14. The width of the tube along the axis of the inductor:

$$a = \frac{l_{\text{ind}} * k_з}{\omega + 1}$$

where $k_з$- the fill factor, which takes into account the presence of electrical insulation between the turns, is usually taken equal to 0.8.

$$a = \frac{40 * 0{,}8}{34 + 1} \approx 1\text{cm} = 10\text{mm}$$

15. Tube wall thickness:

$$b = 1{,}35 * \Delta_{\text{ind}} = 1{,}35 * 1 = 1{,}35 = 135 \text{ mm.}$$

16. The radial height of the tube is calculated after determining the cross-sectional area S of the tube, sufficient to pass the required amount of water:

$$S = \frac{P_u * (1 - \eta)}{4{,}18 * \upsilon * (T_1 - T_0)},$$

where υ – the speed of water movement along the inductor tube (at a pressure of 1.5–2 atm, it is assumed to be 120 cm / s)

T_0 - temperature of water entering the inductor 18°C;

T_1 - leaving water temperature 40°C.

$$S = \frac{121 * 10^3 * (1 - 0{,}72)}{4{,}18 * 120 * (40 - 18)} = 2{,}8 \text{ cm}^2$$

The height of the tube when water passes through all turns of the inductor in series:

$$h = \frac{S}{a-2*b} + 2 * b = \frac{28}{10-2*13,5} + 13.5 * 2 \approx 25 \text{ mm}.$$

Thus, the inductor coil is made from a tube with external cross-sectional 10×25 dimensions and a wall thickness of 13.5 mm. It is not possible to make a coil with such parameters, therefore, a higher frequency should be chosen and the same calculations should be carried out.

A frequency of 500 Hz, at which $\Delta_{\text{ind}} = 3$ mm and $\Delta_{\text{wor}} = 22$ mm. But at this frequency, heating will take longer, about 300 seconds.

17. Net power required to heat the workpiece to the final temperature:

$$P_{\text{billet}} = \frac{g*c_{\text{м}}*(t_{\text{м}}-20)}{0,24*\tau} = \frac{12,3*0,17*1200}{0,24*300} = 34,85\text{kW}$$

18. Active resistance of the inductor:

$$R_1 = \rho_1 * \frac{\pi*d_{\text{ind}}}{l_{\text{ind}}\Delta_{\text{ind}}} = 1,9 * 10^{-6} * \frac{3,14*25}{4*0,3} = 124,29 * 10^{-6}\text{ohm}$$

19. Active resistance introduced by the heated workpiece:

$$R_2 = 6,2 * 10^{-8} * f * \frac{d_{\text{wor}^2}}{l_{\text{wor}}} * \text{A} = 6,2 * 10^{-8} * 500 * \frac{20^2}{2,4} * 0,1 = 516.66 * 10^{-6}\text{ohm}$$

p coefficient:

$$p = \frac{\sqrt{2}}{2} * \frac{20}{2,2} = 12,7$$

In this case, the functions A and B will be equal to 0.

20. Inductor reactance:

$$X_1 = 6,2 * 10^{-8} * f * \frac{d_{\text{ind}^2}}{lind} = 6,2 * 10^{-8} * 500 * \frac{25^2}{4} = 4843,75 * 10^{-6}\text{ohm}$$

21. The reactance introduced by the heated work piece:

$$X_2 = 6,2 * 10^{-8} * f * \frac{d_{\text{заг}^2}}{l_{\text{заг}}} * (1 - \text{B}) = 6,2 * 10^{-8} * 500 * \frac{20^2}{2,4} * 0,9 = 4650 * 10^{-6}\text{ohm}$$

22. Equivalent active and reactance of the inductor, referred to one turn:

$$R_{\text{э}} = R_1 + R_2 = 124,29 * 10^{-6} + 516,66 * 10^{-6} = 640,9 * 10^{-6}\text{ohm}$$

$$X_{\text{э}} = X_1 + X_2 = 4843,75 * 10^{-6} + 4650 * 10^{-6} = 9493,75 * 10^{-6}\text{ohm}$$

23. The total resistance of the inductor, referred to one turn:

$$z' = \sqrt{R_{\text{э}^2} + X_{\text{э}^2}} = \sqrt{(640,9 * 10^{-6})^2 + (9493,75 * 10^{-6})^2} = 9515,35 * 10^{-6}\text{ohm}$$

24. Inductor power factor:

$$\cos\varphi = \frac{R_{\text{э}}}{z'} = \frac{640,9 * 10^{-6}}{9515,35 * 10^{-6}} = 0,07$$

25. Electrical efficiency inductor:

$$\eta_{\text{э}} = \frac{R_2}{R_{\text{э}}} = \frac{516,66 * 10^{-6}}{640,9 * 10^{-6}} = 0,8$$

26. Full efficiency:

$$\eta = \eta_{\text{э}} * \eta_t = 0,8 * 0,9 = 0,72$$

$$P_u = \frac{P_н}{\eta} = \frac{34,85}{0,72} = 45,85 \text{ kW}$$

27. Power supplied to the inductor:

$$\omega = \frac{u}{z'} * \sqrt{\frac{R_э * 10^{-3}}{P_u}} = \frac{750}{9515,35 * 10^{-6}} * \sqrt{\frac{640,9 * 10^{-6} * 10^{-3}}{45,85}} = 9 \text{ turn}$$

28. Inductor current:

$$I_u = \frac{u}{\varpi^2 * z'} = \frac{750}{9^2 * 9515,35 * 10^{-6}} = 973,12 \text{ A}$$

29. Tube width along the inductor axis:

$$a = \frac{l_{\text{ind}} * k_з}{\omega + 1} = \frac{40 * -0,8}{9+1} = 32 \text{ mm}$$

Tube wall thickness:

$$b = 1,35 * Δ_{инд} = 1,35 * 0,3 = 4 \text{ mm}$$

Radial tube height and sectional area S of the tube:

$$S = \frac{P_u * (1 - \eta)}{4,18 * v * (T_1 - T_0)} = \frac{45,85 * 10^3 * 0,28}{4,18 * 120 * 22} = 1,1 \text{ cm}^2$$

$$h = \frac{S}{a - 2 * b} + 2 * b = \frac{9}{32 - 8} + 8 \approx 8,3 \text{ mm}$$

It is advisable to divide the inductor coil into three cooling branches, then:

$$a = \frac{32}{3} \approx 10,6 \text{mm}.$$

At a frequency of 500 Hz, the coil is made with external dimensions of $10,6 \times 8,3$mm and a wall thickness of 4 mm. Rectangular tubes are obtained by drawing from round tubes of equal section perimeter.

Current density:

$$\delta = \frac{I_u}{a * Δ_{\text{ind}}} = \frac{973,12}{32 * 3} = 10,1 \text{ a/mm}^2$$

Generator current:

$$I_г = I_u * \cos\varphi = 973,12 * 0,07 = 68,11 \text{ A}$$

30. Reactive power of the capacitor bank:

$$P_c = \frac{P_u}{\cos\phi} = \frac{45,85}{0,07} = 655 \text{ kvar}$$

The number of banks of a capacitor bank with a reactive power of one capacitor type EMV:

0.75 / 1.5 - 2.5, 125 kvar

$$N_c = \frac{655}{125} \approx 5 \text{ pieces}$$

The heated workpiece has dimensions: = 200 mm and lengths of the hardened part = 24 mm, workpiece weight g = 12.3 kg, made of 40X steel. To calculate the inductor, the current frequency is preselected from Table 1.

Table 1. Standard values of frequencies for cylindrical blanks

Standard current frequency, Hz	Radio frequency	8000	2500	1000	500	50
Workpiece diameter, mm	before 20	15 - 40	30 - 80	50 -120	70 - 160	150 and more

In this case, a frequency of 50 Hz is suitable for the inductor, and we select it as the final one. In this case, the generator voltage will be 750 V. The heating time for a part with such a diameter, at such a frequency, will be about 120 seconds.

The inner diameter of the coil of the inductor:

$$d_{\text{ind}} = d_{\text{wor}} + 50 = 200 + 50 = 250$$

50 mm is left for the thermal insulation and the gap between the thermal insulation and the workpiece. A significant increase in the diameter of the coil of the inductor in comparison with the diameter of the workpiece reduces the efficiency. installation. Thermal efficiency under the considered conditions can be taken equal to 0.9.

2. The length of the coil of the inductor will be determined depending on the heating time, the productivity of the installation and the design features of the part. The length of the inductor will be 40 mm. It is required to calculate the inductor for heating the "stator" part. The heated workpiece has dimensions:

d_{blank} = 200 mm and lengths of the part to be hardened = 24 mm, workpiece weight g = 12.3 kg, made of 40X steel. To calculate the inductor, the current frequency is preselected from Table 1.

In this case, a frequency of 50 Hz is suitable for the inductor, and we select it as the final one. In this case, the generator voltage will be 750 V. The heating time for a part with such a diameter, at such a frequency, will be about 120 seconds.

Conclusions

For simplify and facilitate the process of hardening by high frequency currents of the "stator" part, a spray-cooled inductor with a sectional design was developed.

In this case, a frequency of 50 Hz is suitable for the inductor, and we select it as the final one. In this case, the generator voltage will be 750 V. The heating time for a part with such a diameter, at such a frequency, will be about 120 seconds.

References

[1] Development of the theory and practice of metallurgical technologies: in 3 volumes / VN Peretyatko [and others]; under the editorship of V. N. Peretyatko, E. V. Protopopov, I. F. Selyanin. - M.: Teplotekhnik, 2010 -. T. 2: Plasticity and destruction of steel in heating and pressure treatment: monograph. - M., 2010. - 351 p.
[2] Sharaya O. A. Theory and technology of heat treatment in situational, expert games and tasks. - Karaganda: KSTU, 2010. - 78 p.
[3] Kanaev A.T. Technology of heat treatment of metallic materials: the textbook is designed for students specializing in materials science. - Astana: Arman-PV, 2013. - 388 p.
[4] Materials of construction and heat treatment. Laboratory workshop: a textbook for students. - Karaganda: KSTU, 2015. - 92 p.
[5] Isin D. K. Structural materials and heat treatment. - Karaganda: KSTU, 2017. – 234 p.
[6] Installations of induction heating: textbook / ed. A.E. Slukhotskiy - Leningrad: Energoizdat, 1981. - 328 p.
[7] Slukhotskiy A.E. Inductors for induction heating. - Leningrad: Energy, 1974. - 264 p.

Information of the authors

Malashkevichute – Brillant Elena Iozasovna, senior lecturer of the department “Nanotechnology and Metallurgy” of Karaganda Technical University
E-mail: elenei66@mail.ru

Medvedeva Irina Evgenievna, senior lecturer of the department “Nanotechnology and Metallurgy” of Karaganda Technical University
E-mail: mama12344@mail.ru

Tulegenova Sholpan Nygmetovna, senior lecturer of the department “Nanotechnology and Metallurgy” of Karaganda Technical University
E-mail: sholpan.tulegenova.65@mail.ru

DOI 10.52209/2706-977X_2022_1_10 **IRSTI 55.31.35** **UDC 620.178.38**

Abrasive Reinforced Wheel Strength

Abrashkevich Y.[1*], Machishin G.[1], Marchenko A[1],
Balaka M.[1], Zhukova Ye.[1], Shestakov V.[2]
[1]Kiev National University of Civil Engineering and Architecture, Kiev, Ukraine,
[2]Ural State Mining University, Ekaterinburg, Russia
*corresponding author

Abstract. The purpose of the work is to develop a mathematical model for calculating the stress-strain state of abrasive reinforced wheels. It will allow determining the stress in the wheel, taking into account the effect of the reinforcing mesh. Stresses occur when performing cutting and stripping operations. Mechanical strength of unreinforced abrasive wheels is determined by centrifugal and bending forces. Their distribution during reinforcement is unknown. It has been established that an abrasive reinforced wheel is an anisotropic body. Anisotropy can be reduced by offsetting reinforcing meshes of one relative to the other by an angle of 45^0. The paper develops a mathematical model of the stress-strain state of an abrasive reinforced wheel. The mathematical model takes into account anisotropy of the abrasive reinforced wheel properties. To determine the centrifugal force there can be used the formulas of the elasticity theory for an orthotropic body. The plate is rigidly fixed on the inner contour. Stresses are experimentally determined in the wheel. Stresses arise from the action of centrifugal and bending forces. They are comparable with tensile strength of the matrix of a wheel and reach 8–23 MPa. The developed mathematical model of the strength characteristics of abrasive reinforced wheels allows calculating the efforts that occur in a wheel. This makes it possible to predict their reliability and safe operation.

Keywords: reinforced abrasive wheel, centrifugal and bending forces, deformations, reinforcing mesh, strength.

Introduction

Cutting and cleaning abrasive reinforced wheels are widely used not only in construction but also in mechanical engineering, instrument making, and other sectors of the national economy associated with metal treatment. The annual consumption of wheels amounts to hundreds of millions pieces, so only the Luga Abrasive Plant produces more than 300 million pieces per year [1, 2]. Abrasive reinforced wheels operate in combination with manual and portable machines [3] with the working speed of 80 m/s and are classified as high-risk tools [4]. At present, quite a lot of work has been done at studying the processes in the field of metal grinding [5, 6]. There are practically no works aimed at increasing the mechanical strength of abrasive reinforced wheels, which are widely used in cutting and cleaning operations. At the same time, there is work [7] that presents the results of experimental studies to determine stresses that arise in the wheel during operation. In this paper, for the first time, the issues related to the impact of forces acting on wheels during operation, as well as the impact of reinforcement on its strength indicators, are considered.

The purpose of the work is to develop a mathematical model for calculating the stress-strain state of abrasive reinforced wheels, which will allow determining stresses that take into account the impact of the reinforcing mesh that occur during cutting and grinding operations.

1. Methodology

The worker's safety is determined by the abrasive reinforced wheel strength that during operation is in the complex stress-strain state as a result of centrifugal, bending, tangential and normal forces.

When rotating in a wheel there arise centrifugal accelerations $a = 3 \cdot 10^4 - 20 \cdot 10^4$ м/сек^2 that lead to the appearance of tensile stresses on the inner contour of the wheel that are comparable in magnitude to the material tensile strength.

Bending forces constantly act on cleaning wheels and can also appear in cutting wheels when they are distorted or pinched [8, 9]. For a cleaning wheel, bending forces can be represented by a concentrated force F_{izg} (Figure 1) that is applied to the cutting edge of the wheel perpendicular to its plane, and is equal in magnitude to the force P with which the operator presses the wheel to the cutting surface multiplied by the sine of the wheel inclination angle α. Stresses caused by bending forces on the inner contour can also reach values comparable to wheel material tensile strength.

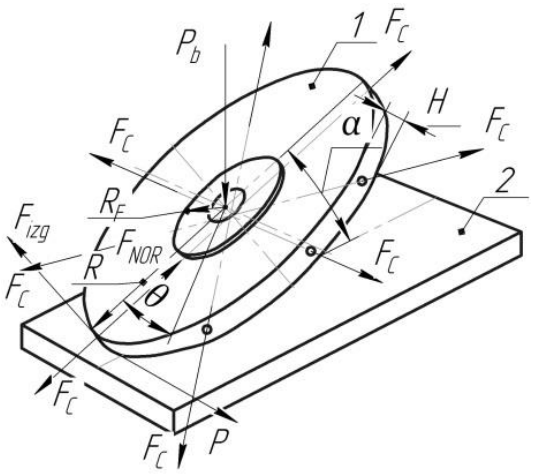

Fig. 1. – Forces acting on the grinding wheel

The analysis performed shows that even in the area of the clamping flange, stresses caused by tangential and normal forces are much lower than its material tensile strength and can be ignored.

Mechanical strength of the wheels is determined by the centrifugal forces that occur during its rotation. In this regard, for an approximate analysis of the stress state and for comparison of experimental data, the usual formulas of the elasticity theory are used supposing that the wheel is an isotropic body.

The equilibrium equation for an elastic wheel that rotates with an angular velocity ω and a constant thickness has the form [10, 11]:

$$\frac{d}{dr}\left[\frac{1}{r}\cdot\frac{d(UR)}{dR}\right]=-\frac{1-\nu^2}{E}\cdot\rho\cdot\omega^2\cdot R, \tag{1}$$

where U is the radial movement of the point that is at the *R* distance from the wheel center, m;

E is the elasticity modulus of the wheel material, Pa;

ν is the Poisson coefficient;

ρ is the material density, kg/cm^3;

g is the gravitational acceleration in the accepted systems of units.

By double integrating equation (1) and by denoting $\tilde{a}_0=\frac{1}{8}\cdot\rho_{kr}\cdot\omega^2$, we obtain:

$$U=A_1\frac{1-\nu}{E}\cdot R+A_2\frac{1+\nu}{E}\cdot\frac{1}{R}-\tilde{a}_0\cdot\frac{1-\nu^2}{E}\cdot R^3, \tag{2}$$

where A_1, A_2 are integration constants that are determined from the boundary conditions.

Stresses in the radial σ_r and angular σ_θ directions that correspond to movements (2), according [11], have the form:

$$\begin{aligned}\sigma_r&=A_1-A_2\frac{1}{R^2}-\tilde{a}_o\cdot(3+\nu)R^2,\\ \sigma_\theta&=A_1+A_2\frac{1}{R^2}-\tilde{a}_o\cdot(1+3\nu)R^2.\end{aligned} \tag{3}$$

The boundary conditions on the inner and outer contours are accepted as follows:

$$\left.\begin{aligned}\sigma_r\big|_{R=R_0}&=0;\\ U_r\big|_{R=R_F}&=0.\end{aligned}\right\} \tag{4}$$

The boundary conditions take into account the rigid fixation of the wheel along the contour of the clamping flange and the absence of stresses on the cutting edge.

The integration constants A_1, A_2 are determined from the following system of equations:

$$\begin{aligned}A_1\frac{1-\nu}{1+\nu}\cdot R_F^2+A_2&=\tilde{a}_0(1-\nu)R_F^4,\\ A_1\cdot R_0^2-A_2&=\tilde{a}_0(3+\nu)R_0^4.\end{aligned} \tag{5}$$

After transformations we have:

$$A_1 = \tilde{a}_0 \frac{(1-\nu)\cdot R_F^4 + (3+\nu)\cdot R_0^4}{\frac{1-\nu}{1+\nu}\cdot R_F^2 + R_0^2},$$
$$A_2 = \tilde{a}_0 (1-\nu) R_F^2 \cdot R_0^2 \frac{R_F^2 - \frac{(3+\nu)}{1+\nu}\cdot R_0^2}{\frac{1-\nu}{1+\nu} R_F^2 + R_0^2}. \quad (6)$$

Now, using formula (3), it is easy to calculate the stresses in the wheel. At this, the inner contour ($R=R_F$) that is the most probable site of failure, is of special interest.

It should be noted that in the case when, under the impact of some overloads, the material of the wheel matrix is destroyed, the stress-strain state in the wheel undergoes significant changes. At this, its integrity under the action of centrifugal forces can be maintained only by means of a reinforcing mesh that is able to resist only radial forces.

In work [12], it is proposed to place grids (Figure 2) of a specified configuration, which will improve the technical characteristics of the wheel.

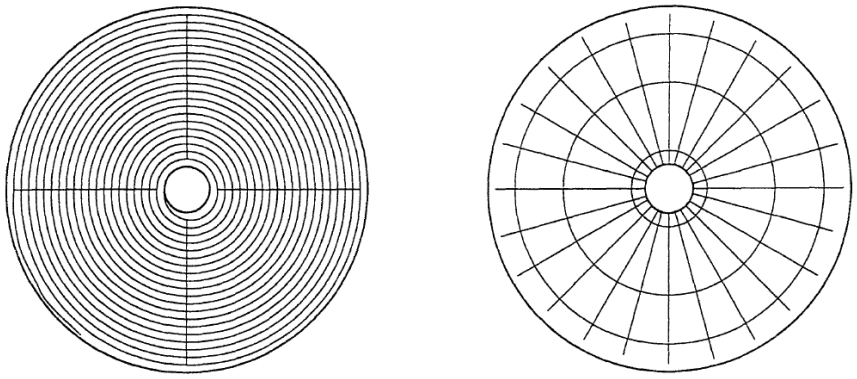

a) b)

a) tangential; b) radial

Fig. 2. – The proposed wheel reinforcement schemes

Let x is the relative volumetric content of reinforcing fibers in the body of the wheel. Then, considering the balance of the circle element and assuming that $\sigma_\theta = 0$ and the radial stress is perceived only by favorably oriented fibers, the proportion of which adds up q_1 a part of all the fibers ($q_1=1/2$), we have:

$$\frac{d\sigma_r}{dR} + \frac{\sigma_r}{R} = -\frac{1}{q_1 x}\cdot \rho_{kr}\omega^2 R. \quad (7)$$

Expressing stress through the movement, we obtain:

$$\frac{d^2U}{dR^2} + \frac{1}{R}\cdot\frac{dU}{dR} = -\frac{1}{E_C}\cdot\frac{1}{q_1 x}\rho_{kr}\omega^2 R. \quad (8)$$

where E_C is the elasticity modulus of the reinforcing mesh material.

The general integral of equation (8) has the form:

$$U = C_1 \ln R + C_2 - \frac{\omega^2 \rho_{kr}}{3E_C q_1 x} R^3, \quad (9)$$

from here

$$\sigma_r = E_C C_1 \cdot \frac{1}{R} - \frac{\omega^2 \rho_{kr}}{3q_1 x} R^2, \quad (10)$$

taking into account that $\sigma_r\big|_{R=R_0} = 0$, we determine:

$$C_1 = \frac{\omega^2 \rho_{kr} R_0^3}{3E_C q_1 x}, \quad (11)$$

and substituting (11) into (10), we find the expression for stresses in the reinforcing fibers on the inner contour:

$$\sigma_r = \frac{\omega^2 \rho_{kr} \left(R_o^3 - R_F^3 \right)}{3 q_1 x R_F}. \tag{12}$$

In the conditions of the wheel acceleration (braking) the angular acceleration $a_{okr} = \frac{dV_P}{dt} = R\frac{d\omega}{dt}$ causes in the $R = const$ sections stresses σ_r that can be determined from the condition of equilibrium of the wheel part that is between the R and R_0 radii:

$$\sigma_r \cdot 2\pi \cdot R_F^2 \cdot \tilde{H} = \rho_{kr} \cdot \tilde{H} \cdot 2\pi \int_{R_F}^{R_0} \frac{d\omega}{dt} R^3 dR,$$

$$\sigma_r = \frac{\rho_{kr}}{4} \cdot \frac{d\omega}{dt} \cdot \frac{R_0^4 - R_F^4}{R_F^2}. \tag{13}$$

After testing the samples of the wheel for tension, the obtained experimental and calculated values of stresses in the angular and radial directions have been compared.

It has been established that the calculated stresses are more than 2 times lower than the experimental ones, that is, they can only be used for qualitative assessments.

For the further analysis on a special bench, the deformations that occur in wheels with different reinforcement schemes under the action of centrifugal forces were determined. It was confirmed that in the directions coinciding with the mesh fibers, the magnitude of the deformations is 1.3–1.6 times lower. At this, maximum and minimum strengths are, respectively, for specimens in which the direction of tensile forces coincides with the direction of the fibers of the reinforcing mesh or makes 45^0 with them (Figure 3). It has been established that depending on the design, the abrasive reinforced wheel tensile strength is 8–23 MPa.

After studying the stress-strain state, the wheels on the bench have been brought to destruction that has ocurred mainly along the radii. Thus, it has been established that the abrasive reinforced wheel is an anisotropic body, while orthotropy of its mechanical properties is observed. Anisotropy can be reduced if the reinforcing meshes are arranged in such a way that the fibers of one of them are displaced by the angle of 45^0 relative to the fibers of the other one. At this, the wheel is the most equal in strength and its reliability increases. Changing the orientation of the internal meshes of the abrasive reinforced wheels (Figure 3) makes it possible to increase their tensile strength by an average of 20% and they can be considered as orthotropic bodies.

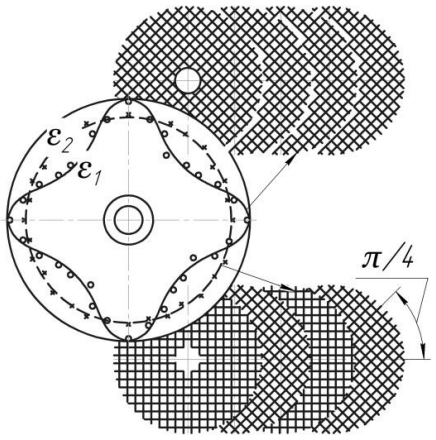

Fig. 3. – Diagram of the deformation distribution in the wheels with different orientation of reinforcing meshes

Changing the elasticity modulus of the wheel material that is an anisotropic body, is described by the dependence:

$$E(\theta) = \frac{E_1 E_2}{E_1 \cos^4\theta + (\frac{4E_1E_2}{E_{12}} - E_1 - E_2)\sin^2\theta\cos^2\theta + E_2 \sin^4\theta}, \tag{14}$$

where E_1, E_2, E_{12} are elasticity moduli for tension in the directions making with the reinforcing mesh fibers the angles $\pi/2, \pi, \pi/4$.

For an orthotropic wheel rotating with an angular velocity ω, the distribution of stresses under the action of centrifugal forces will be obtained using the stress function:

$$\begin{aligned}&\frac{1}{E_\theta}\frac{\partial^4 F_c}{\partial R^4}+(\frac{1}{G_{r\theta}}-\frac{2\nu_r}{E_r})\frac{1}{R^2}\frac{\partial^4 F_c}{\partial R^2\partial\theta^2}+\frac{1}{E_r}\frac{1}{R_4^4}\frac{\partial^4 F_c}{\partial\theta^4}+\\&+\frac{2}{E_\theta}\frac{1}{R}\frac{\partial^3 F_c}{\partial R^3}-(\frac{1}{G_{r\theta}}-\frac{2\nu_r}{E_r})\frac{1}{R^3}\frac{\partial^3 F_c}{\partial r\partial\theta^2}-\frac{1}{E_r}\frac{1}{R^2}\frac{\partial^2 F_c}{\partial R^2}+\\&+(2\frac{1-\nu_r}{E_r}+\frac{1}{G_{r\theta}})\frac{1}{R^4}\frac{\partial^2 F_c}{\partial\theta^2}+\frac{1}{E_r}\frac{1}{R^3}\frac{\partial F_c}{\partial R}=\\&=-\left[\frac{1-\nu_\theta}{E_\theta}\frac{\partial^2}{\partial R^2}+\frac{1-\nu_r}{E_r}\frac{1}{R^2}\frac{\partial^2 J}{\partial\theta^2}+(\frac{2}{E_\theta}-\frac{1-\nu_r}{E_r})\frac{1}{R}\frac{\partial J}{\partial R}\right],\end{aligned} \tag{15}$$

where E_r, E_θ are the elasticity moduli for tension in the main directions R and θ, Pa; $J=-\frac{\rho_{kr}\omega^2}{2}R^2$ is the moment of inertia;

$G_{r\theta}$ is the shear modulus for the main directions, Pa.

Taking into account that the load from centrifugal forces is symmetrical, the stress function has the form:

$$F_c=A_0+B_0R^2+CR^{1+K}+DR^{1-K}+\frac{\rho_{kr}\omega^2}{2}(3-K-2\nu_\theta)R^2, \tag{16}$$

where $K=\sqrt{\frac{E_\theta}{E_r}}$; $\nu_r=\nu_\theta=\nu$ is the Poisson coefficient.

Using the expressions known from the elasticity theory:

$$\begin{aligned}&\sigma_r^c=\frac{1}{R}\frac{\partial F_C}{\partial R}+\frac{1}{R^2}\frac{\partial^2 F_C}{\partial\theta^2}+J,\\&\sigma_\theta^c=\frac{\partial^2 F_C}{\partial R^2}+J,\\&U_r=R(\frac{\sigma_\theta^c}{E_\theta}-\frac{\nu_r}{E_r}\sigma_r^c).\end{aligned} \tag{17}$$

let's determine the stress components and the movement projections:

$$\sigma_r^c=C(1+K)R^{K-1}+D(1-K)R^{-K-1}-\rho_{kr}\omega^2\frac{3+\nu_\theta}{9-K^2}R^2, \tag{18}$$

$$\sigma_\theta^c=C(1+K)KR^{K-1}+D(1-K)KR^{-K-1}-\rho_{kr}\omega^2\frac{K^2+3\nu_\theta}{9-K^2}R^2, \tag{19}$$

$$U_r^c=\frac{C}{E_\theta}(1+K)(K-\nu_\theta)R^K+\frac{D}{E_\theta}(1-K)R^{-K}-\frac{\rho_{kr}\omega^2}{E_\theta}\frac{K^2-\nu_\theta^2}{9-K^2}. \tag{20}$$

The C and D constants are determined from the boundary conditions:

$$\begin{cases}U_r^c\big|_{R=R_F}=0,\\ \sigma_r^c\big|_{R=R_0}=0.\end{cases} \tag{21}$$

$$C=\frac{\begin{vmatrix}\rho_{kr}\omega^2\frac{K^2-\nu_\theta^2}{9-K^2}R_F^3 & (K-1)(K-\nu_\theta)R_F^{-k}\\ \rho_{kr}\omega^2\frac{3+\nu_\theta^2}{9-K^2}R_0^2 & (1-K)R_0^{-K-1}\end{vmatrix}}{(1-K^2)\left[R_F^KR_0^{-K-1}(K-\nu_\theta)+R_F^KR_0^{K-1}(K+\nu_\theta)\right]}, \tag{22}$$

$$D=\frac{\begin{vmatrix}(1-K)(K-\nu_\theta)R_F^k & \rho_{kr}\omega^2\frac{K^2-\nu_\theta^2}{9-K^2}R_F^3\\ (1+K)R_0^{K-1} & \rho_{kr}\omega^2\frac{3+\nu_\theta^2}{9-K^2}R_0^2\end{vmatrix}}{(1-K^2)\left[R_F^KR_0^{-K-1}(K-\nu_\theta)+R_F^{-K}R_0^{K-1}(K+\nu_\theta)\right]}.$$

Taking into account (22), dependences (18), (19) describe the stressed state of the rotating abrasive reinforced wheel.

2. Results and discussion

In the process of experimental verification of theoretical calculations, there have been determined physical and mechanical characteristics of the wheels (Table 1) with different reinforcement schemes.

Table 1. Physical and mechanical characteristics of wheels

Wheel types	E_1 MPa	E_2 MPa	$E_{1,2}$ MPa	ν	Ultimate tensile strength, σ MPa	Angular breaking speed, ω s^{-1}
41–400×4×32 (one mesh) For cutting mining rocks	4394	4725	3855	0.2	7.4	602
41–300×3×32 (two meshes) For cutting metals	9550	11040	9124	0.2	18.5	760
27–230×6×22,23 (four meshes) For cleaning metals	10440	10870	9540	0.2	23	1060

The total stresses arising in brittle bodies are calculated by the formula $\sigma_{sum}^c = \sigma_r^U - \nu\sigma_\theta^c$. Based on this, the condition for maintaining the integrity of the wheel under the action of centrifugal forces:

$$\sigma_{sum}^c = \sigma_r^c - \nu\sigma_\theta^c \le k_{zp}\sigma_0. \tag{23}$$

Figure 4 shows the dependence σ_{sum}^c on the angular velocity that has been recorded during the wheel destruction. The K, L, M points marked on the curves correspond to the destruction of the wheels. A comparison of calculated and experimental data shows that their ratio does not exceed 8%.

When calculating the stress state that occurs under the action of bending forces, the wheel can be considered as a closed annular plate that is clamped along the inner contour and loaded with a concentrated force along the outer contour.

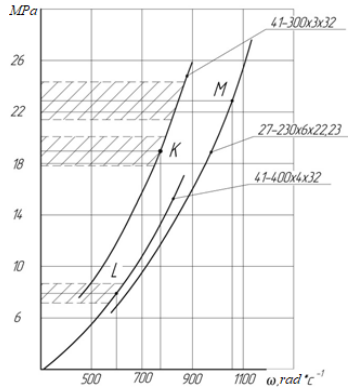

Fig. 4. – Stress changing dependence on the angular speed

It is known [11] from the method of calculating stresses that arise in a wheel under the action of centrifugal forces, the differential equation of bending in polar coordinates has the form [13]:

$$D\Delta FW = 0, \tag{24}$$

where $D = \dfrac{E\tilde{H}^3}{12(1-\nu^2)}$ is cylindrical rigidity, Nm;

$\tilde{H}$ is the plate thickness, m;

E is the elasticity modulus, Pa;

ν is the Poisson coefficient;

W is flexure, m;

$\Delta F = \dfrac{\partial^2}{\partial R^2} + \dfrac{1}{R}\dfrac{\partial}{\partial R} + \dfrac{1}{R^2}\dfrac{\partial^2}{\partial\theta^2}$ is the Laplace second order operator.

The internal forces in the plate (Figure 3) are expressed through the flexure in such a way:

$$M_r = -D\left[\frac{\partial^2 W}{\partial R^2} + \frac{\nu}{R}\left(\frac{\partial W}{\partial R} + \frac{1}{R}\frac{\partial^2 W}{\partial \theta^2}\right)\right], \tag{25}$$

$$M_\theta = -D\left[\nu\frac{\partial^2 W}{\partial R^2} + \frac{1}{R}\frac{\partial W}{\partial R} + \frac{1}{R^2}\frac{\partial^2 W}{\partial \theta^2}\right], \tag{26}$$

$$M_{r\theta} = (1-\nu)D\left[\frac{1}{R}\frac{\partial^2 W}{\partial R\partial\theta} - \frac{1}{R^2}\frac{\partial^2 W}{\partial \theta^2}\right], \tag{27}$$

$$V_r = Q_r - \frac{1}{R}\frac{\partial M_{r\theta}}{\partial \theta} = -D\left[\frac{\partial}{\partial R}\triangle W + (1-\nu)\frac{\partial^2}{\partial R\partial\theta}\left(\frac{1}{R}\frac{\partial W}{\partial \theta}\right)\right], \tag{28}$$

where M_r, M_θ, $M_{r\theta}$, M_r are bending moments, Nm;

Q_r is the transverse force, N;

V_r is the bearing reaction oer unit of the plate contour length, N/m.

The maximum stresses are achieved in each section on the plate surface and are expressed in terms of internal forces using the relations:

$$\begin{aligned}\sigma_r^{izg} &= \frac{6M_r}{\tilde{H}^2},\\ \sigma_\theta^{izg} &= \frac{6M_\theta}{\tilde{H}^2},\\ \sigma_{r\theta}^{izg} &= \frac{6M_{r\theta}}{\tilde{H}^2}.\end{aligned} \tag{29}$$

Solution of equation (24) is expedient to find in the form of the Fourier series [14]:

$$W = F_0(R) + \sum_{m=1}^{\infty} F_m(R)\cos m\theta, \tag{30}$$

where $F_m(R)$ is the function of the R constant that is determined by substituting (30) into equation (24) and has the form:

$$F_0(R) = A_0 R + B_0 R^2 + C_0 \ln R + D_0 R^2 \ln R, \tag{31}$$

$$F_1(R) = A_1 R + B_1 R^{-1} + C_1 R^3 + D_1 R \ln R, \tag{32}$$

$$F_m(R) = A_m R^m + B_m R^{-m} + C_m R^{m+2} + D_m R^{-m+2}, \tag{33}$$

where A_m, B_m, C_m, D_m ($m = 0, 1, 2, \ldots$) are arbitrary constants that are determined in the case considered from the following boundary conditions:

$$W\big|_{R=R_F} = 0. \tag{34}$$

$$\left.\frac{dW}{dR}\right|_{R=R_F} = 0. \tag{35}$$

$$M_r\big|_{R=R_0} = 0. \tag{36}$$

$$V_r\big|_{R=R_2} = \frac{F_{izg}}{\pi R_0^2}\left(1 + \sum_{m=1}^{\infty}\cos m\theta\right). \tag{37}$$

Having made the needed operations of differentiation on series (30), we obtain an expansion in the Fourier series for the functions $\frac{dW}{dR}(R,\theta)$, $M_r(R,\theta)$, $V_r(R,\theta)$, $M_\theta(R,\theta)$, $M_{r\theta}(R,\theta)$:

$$\frac{dW}{dR} = \varphi_0(R) + \sum_{m=1}^{\infty} \varphi_m(R)\cos m\theta, \tag{38}$$

$$M_r = \mu_0(R) + \sum_{m=1}^{\infty} \mu_m(R)\cos m\theta, \tag{39}$$

$$V_r = \nu_0(R) + \sum_{m=1}^{\infty} \nu_m(R)\cos m\theta, \tag{40}$$

$$M_\theta = \psi_0(R) + \sum_{m=1}^{\infty} \psi_m(R)\cos m\theta, \tag{41}$$

$$M_{r\theta} = \eta_0(R) + \sum_{m=1}^{\infty} \eta_m(R)\cos m\theta, \tag{42}$$

where φ_m, μ_m, ν_m, ψ_m, η_m are the functions that include arbitrary constants.

Taking into account (38–42) and (30), boundary conditions (34–37) are reduced to the following systems of linear equations in the unknowns A_m, B_m, C_m, D_m ($m = 0, 1, 2, \ldots$)

$$\begin{aligned} &F_m(R_1) = 0, \\ &\varphi_m(R_1) = 0, \\ &\mu_m(R_2) = 0, \\ &\nu_m(R_0) = \begin{cases} \dfrac{F_{izg}}{2\pi R_0}, & m = 0 \\ \dfrac{F_{izg}}{\pi R_0}, & m \neq 0 \end{cases}. \end{aligned} \tag{43}$$

Having determined from (43) arbitrary constants for each harmonic of series (30), it is possible to calculate the internal forces in the wheel using formulas (25)-(27), and then, using (29), the stresses that are caused by bending.

The results of the various force factors impact are summarized and the main stresses are calculated as follows:

$$\sigma_{sum} = (\sigma_r^c + \sigma_r^{izg}) - \nu(\sigma_\theta^c + \sigma_\theta^{izg}). \tag{44}$$

The developed model of the stress-strain state of the wheel makes it possible to predict its strength characteristics, which will ensure safe and reliable operation.

Conclusions

As a result of theoretical and experimental studies, it has been determined that the abrasive reinforced wheel is an anisotropic body.

The main force factors affecting the abrasive wheel strength are bending and centrifugal forces, while for cleaning wheels, the effect of bending and centrifugal forces should be taken into account, and for cutting wheels the effect of centrifugal forces.

The greatest danger from the point of view of the wheel destruction is its working part at the contour of the clamping flange of the drive machine.

The elasticity moduli of the wheel bond significantly exceed the elasticity moduli of the reinforcing mesh, so it practically does not perceive loads at the initial stage of loading. The role of the reinforcing mesh is reduced to maintaining the integrity of the wheel after the formation of cracks in it.

To increase the wheel strength, it is advisable to reinforce it additionally with small-diameter meshes near the contour of the clamping flange of the drive machine, as well as to increase the dispersion of the elasticity and strength characteristics of the wheel polymer matrix.

The developed algorithm for calculating the strength characteristics of abrasive reinforced wheels allows calculating the forces that occur in the wheel. This makes it possible to predict their reliability and safer operation.

References

[1] Mode of access: http://www.abrasives.ru/news/12/5264/. – Date of access: 10.10.2020. (in Russian).

[2] Interview with Vadim Andreyevich Borisov, Director General of the “Luga Abrasive Plant›” “We cannot be led astray ...”. Mode of access: https://master-forum.ru/intervyu-generalnogo-direktora-171-luzhskogo-abrazivnogo-zavoda-187-vadima-borisova-171-nas-nevozmozhno-sbit-s-puti-187/. – Date of access: 10.10.2020. (in Russian).

[3] Ojolo S.J., Orisaleye J.I., Adelaja A. O. Development of a high speed abrasive cutting machine. Journal of Engineering Research. Vol. 15, No. 3, September, 2010. - P. 1–8.

[4] Test abrasive cutting and grinding wheels: how to hold it? Stand for the test. Mode of access: http://ukrabraziv.com.ua/novosti/33-ispytanie-shlifovalnykh-abrazivnykh-krugov. – Date of access : 10.10.2020. (in English).

[5] Bilek O., Hrdina J., Lukovics I., Pero R., Samek D. Improved shape of rotating grinding wheels for high speed grinding. Tehnički vjesnik. Vol. 21, 2014.- P. 63–68. (in English).
[6] Y. Hou, C. Li and Y. Zhou, "Applications of High-Efficiency Abrasive Process with CBN Grinding Wheel," Engineering, Vol. 2 No. 3, 2010. – P.184-189. doi: 10.4236/eng.2010.23026. (in English).
[7] Mackin Thomas J. Failure analysis of a particulate composite cutoff wheel with fiber reinforcing / T. J. Mackin, H. M. Inglis // Proceedings of the 10th International Conference on Fracture, Honolulu, HI, December 2–6, 2001. Mode of access: http://www.gruppofrattura.it/ocs/index.php/ICF/ICF10/paper/viewFile/4651/6659. Date of access : 30.10.2021. (in English).
[8] Abrashkevych Yu. D., Pelevin L. E., Machyshyn G. M. Exploitation of reinforced abrasive wheels. Installation and special works in construction. Vol. 4 [883], 2016. - P. 30 – 32 (in Russian).
[9] Abrashkevych Yu. D., Pelevin L. E., Machyshyn G. M., Tishkovets V.P. Factors affecting the safety of the use of abrasive reinforced wheels. Installation and special works in construction, Vol. 9 [883], 2017. - P. 11–14 (in Russian).
[10] Timoshenko S.P., Gudier J. Theory of elasticity. Main editorial board of physical and mathematical literature of "Nauka" publishing house, 1975. – 576 p. (in Russian).
[11] Pisarenko G.S. The course of resistance of materials. Textbook. – Kiev: Vishcha School, 1979. – 696 p. (in Russian).
[12] Massachusetts Institute of Technology, Dept. of Materials Science and Engineering, 1996. Includes bibliographical references (p. 104-105). Mode of access: https://www.researchgate.net/publication/33807673_Manufacturing_glass-fiber_reinforcement_for_grinding_wheels. – Date of access: 30.10.2021. (in English).
[13] Timoshenko S.P., Voinovsky-Krieger S. Plates and shells. – M.: Science, 1966. - 636 p.(in Russian).
[14] Mode of access: http://mathprofi.ru/ryady_furie_primery_reshenij.html. – Date of access: 30.10.2021 (in Russian).

Information of the authors

Abrashkevich Yuri Davydovich, doctor of technical sciences, professor of Kiev National University of Civil Engineering and Architecture
E-mail: abrashkevich_yu@mail.ru

Machishin Grigory Mikhailovich, PhD, assistant of Kiev National University of Civil Engineering and Architecture
E-mail: machishin_g@mail.ru

Marchenko A., assistant of Kiev National University of Civil Engineering and Architecture
E-mail: marchenko_a@mail.ru

Balaka M., assistant of Kiev National University of Civil Engineering and Architecture
E-mail: balaka_m@mail.ru

Zhukova Ye., assistant of Kiev National University of Civil Engineering and Architecture
E-mail: zhukova_ye@mail.ru

Shestakov Viktor Stepanovich, candidate of technical sciences, professor of the department of mining machines and complexes of Ural State Mining University
E-mail**:** Shestakov.v.s @mail.ru

DOI 10.52209/2706-977X_2022_1_19 **IRSTI 55.53.29** **UDC 621.878/625.76**

Calculating Design and Mode Parameters of Mine Hydraulic Excavator Working Equipment Mechanisms

Teliman I.[1*], Malybayev N.[1], Bezkorovainy P.[1], Ibrayeva N.[1], Komissarov A.[2]

[1]Karaganda Technical University, Karaganda, Kazakhstan
[2]Ural State Mining University, Ekaterinburg, Russia
*corresponding author

Abstract. It is shown that the main executive mechanisms of the mine hydraulic excavator (mechanisms for turning the boom, turning the handle and turning the bucket) are hydro-mechanical units in which the engines (hydraulic cylinders) are an integral part of the lever-hydraulic mechanisms. The presence of a kinematic connection between the engine (hydraulic cylinder rod) and the members of the lever-hydraulic mechanism determines certain relations between the parameters of the engine and the power parameters implemented on the driven member (boom, handle and bucket): kinematic and dynamic transfer functions. Based on a simulation model of the main mechanisms functioning, expressions for definition of transfer functions have been obtained. It has been established that there are rational values of the dynamic transfer functions of the main mechanisms at which the correspondence between the energy-power parameters realized at the driven members and the mode of loading of the driven members is achieved. Synthesizing the design schemes of the main mechanisms with rational values of dynamic transfer functions will allow excluding an overload of engines and increasing the energy efficiency of the hydraulic excavator functioning.

Keywords: mine hydraulic excavator, main executive mechanisms, kinematic and dynamic transfer functions of mechanisms

Introduction

In the conditions of competitive development of the mining sector of the economy, the problem of improving the quality of technological machines, in particular, the energy efficiency of equipment is of paramount importance.

The scientific foundations and basic principles of the effective functioning of hydraulic excavators as the main type of excavation equipment were developed and formulated in the works by N.N. Melnikov, A.V. Ranev, B.I. Satovsky, V.M. Shteintsaig and other scientists. Further development of the theory of hydraulic excavators was reflected in works [1-11].

In the general case, a preliminary assessment of the equipment energy efficiency can be performed by comparing the specific (related to the performance of the excavator) energy consumption with the theoretical energy intensity of the work process.

However, at this, it is not possible to establish the degree of using the energy resources without establishing the dynamics of the energy-power parameters formation implemented on the working body.

1. Methodology

The carried out studying of the state of the area under consideration, namely the studying of the processes of the operation and analyzing of the leading units of hydraulic excavators breakdowns, revealed that two main areas of the studies can be distinguished:

- analyzing and studying the work processes occurring in the course of the main equipment operation, that is, the working tool pushing into the rock mass;
- developing a mathematical model of the processes occurring in the course of main mechanisms of a hydraulic excavator, as well as formulating and analyzing the dependences between the energy-power parameters and parameters of a hydraulic power plant.

In addition, in work [12] it was shown that the use of loading equipment of a straight shovel type hydraulic excavator made it possible to increase significantly the bucket capacity, due to the possibility of increasing the force on the cutting edge of the working equipment element (bucket). Since the main load is the force of the rock resistance to the bucket pushing into the rock pile, and its value is limited by the force of the excavator running equipment adhesion to the ground, the effect of the mass of the excavator will be significant.

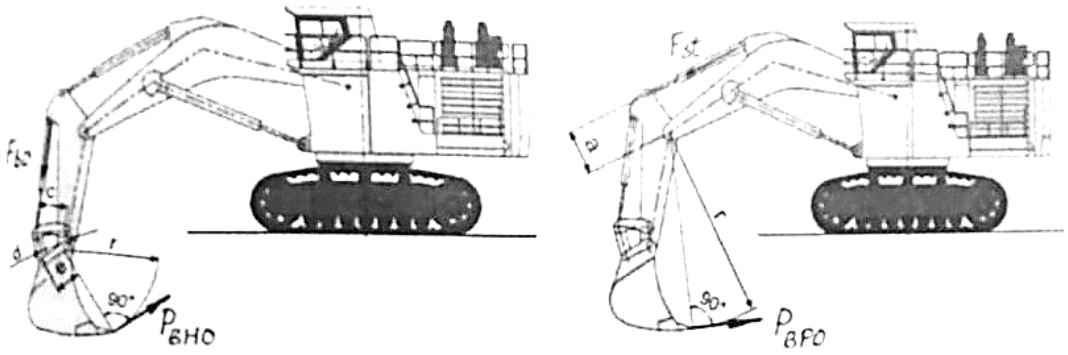

a) b)

a) pushing (breaking out) $P_{вно}$; b) pulling out (separation) $P_{вро}$

Fig . 1. – Kinematic schemes for determining the forces on the teeth of the backhoe bucket

The forces of the backhoe bucket pushing into the massif and pulling the bucket out of the massif (Figure 1) are determined by the following expressions:

$$P_{вно} = \frac{F_{bu} \cdot c \cdot e}{d \cdot r} \quad (1)$$

$$P_{вро} = \frac{F_{sh} \cdot a}{r} \quad (2)$$

where $P_{вно}$ is the force of the backhoe bucket pushing;

$P_{вро}$ is the force of the bucket pulling out;

F_{bu} is the force in the hydro-cylinders of the bucket swing;

F_{sh} is the force in the hydro-cylinders of the stick turn;

a, e, c, d, r are the action shoulders according to the scheme (Figure 1 a) and b))

For a backhoe hydraulic bucket, the implementation of maximum pushing and pulling out forces significantly depends on the angles of the stick swing relative to the hinge of its attachment to the boom and the bucket, relative to the hinge of its attachment to the stick (Figure 2) [13].

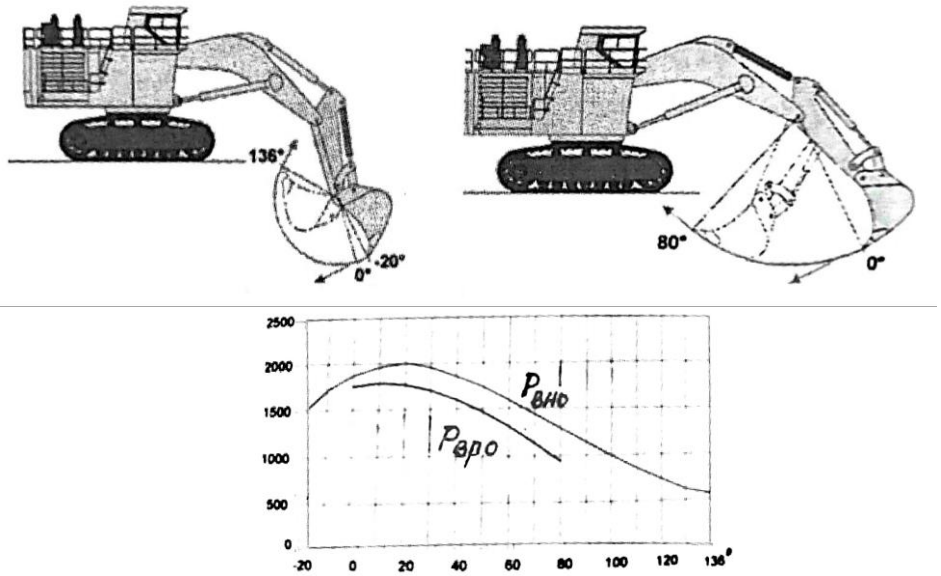

Fig. 2. – Maximum forces of pushing $P_{вно}$ and pulling out $P_{вро}$ dependence on the stick swing angle of excavator PC 8000

The positive characteristics of the machine described above gave a significant impetus to the widespread introduction of hydraulically driven excavators in the mining industry in the far abroad countries.

However, during operation, a number of shortcomings inherent to the loading equipment appeared, such as:

- decreasing the excavator productivity when working in the face with poor-quality preparation of the rock mass, since with inclined and steep lines of motion, the forces on the bucket teeth are significantly reduced;
- increasing the load and weight of the working equipment due to the serial connection of the working mechanisms, i.e. working mechanisms to some extent perceive the load acting on the working equipment;
- sharp increasing the workloads determined by the increased energy intensity of the working process due to extrusion of rock from the massif (Figure 2) causes increasing the engine power of the bucket swinging mechanism and the rated power of the primary engine;
- the forces developed by the excavator while working on fractured and layered rock masses require the use of specialized methods of work, for example, the forces required for pulling out are much lower than the forces required to pushing the bucket into the rock mass. Therefore, it is necessary to make a stop with the front edge of the bucket in the body of the face with the subsequent bucket swinging.

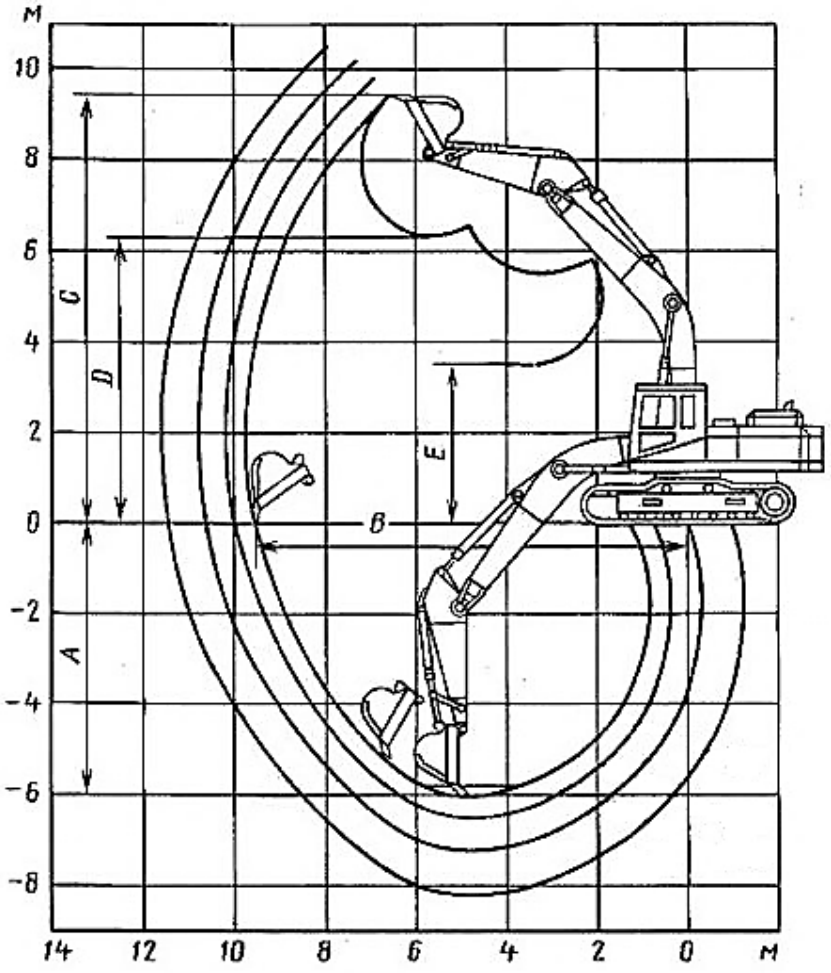

A – max depth; B – max radius; C – digging height; D, E – max and min unloading height

Fig. 3. – Work process

Thus, the characteristic mode of the excavator operation is the joint operation of all the main hydraulic cylinders of the machine. With the constant operation of the machine, a set of rock mass, raising and turning the boom, coordinated work is required (Figure 3).

The object of study is the main mechanisms of the working equipment (mechanisms for turning the boom, swinging the stick and the bucket) of a hydraulic excavator (Figure 4).

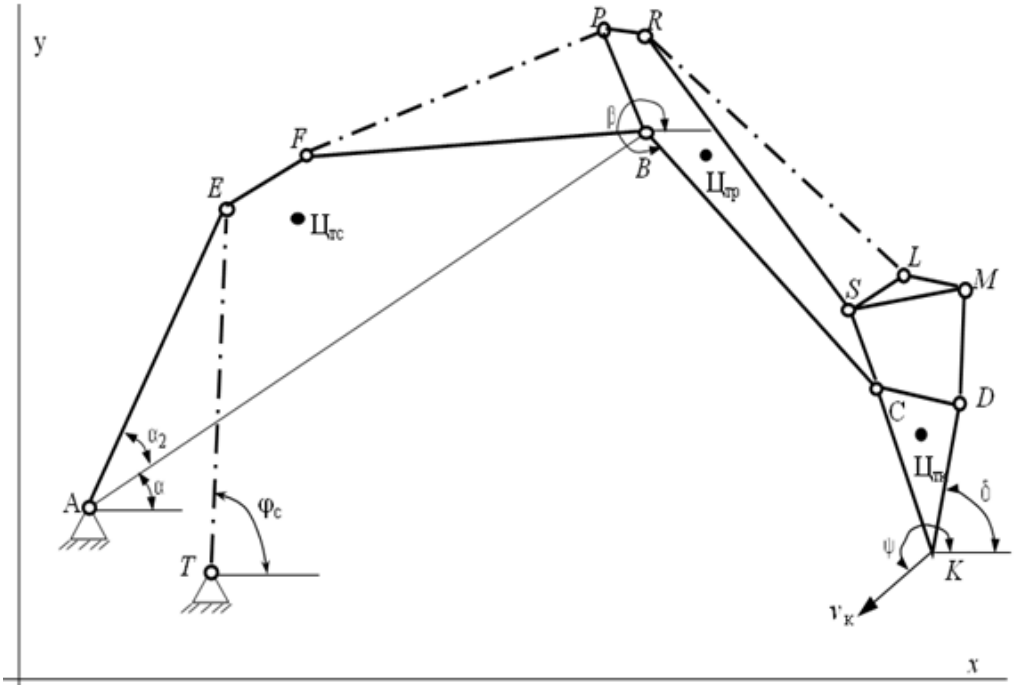

Fig. 4. - Diagram for determining work characteristics of the hydraulic excavator main mechanisms

A feature of the main mechanisms of hydroficated working equipment is the presence of a kinematic connection between the hydraulic motors (hydraulic cylinders) and the members of the mechanisms, since the hydraulic motors themselves (actually the cylinder and the piston with the rod) are the members of the mechanisms.

At this, the ratios between the parameters of the hydraulic motors mechanical energy and the energy-power parameters implemented on the driven members (boom, stick and bucket) depend both on the type of mechanical characteristic of the hydraulic motors and on the type of structural diagram of the mechanisms.

Based on the kinematic and force analysis of the hydraulic excavator main mechanisms [14, 15], the analytical expressions for calculating the kinematic $\Pi\Phi_V$ and force $\Pi\Phi_F$ transfer functions were obtained.

The dependences for determining the transfer functions of the main mechanisms have the form:

$$\Pi\Phi_V = \frac{V_{\text{в.зв}}}{V_{\text{шт}}} = f_1(l_i, \alpha_j) \tag{3}$$

$$\Pi\Phi_F = \frac{F_{\text{в.зв}}}{F_{\text{шт}}} = f_2(l_i, \alpha_j, G_i) \tag{4}$$

where $V_{\text{в.зв}}$ is the speed of the driven member of the mechanism, i.e. the speed of point B of the boom, point C of the stick and point K of the bucket (digging speed), respectively;

$V_{\text{шт}}$ is the speed of the hydro-cylinder rod movement;

l_i is the size (lengths) of the mechanism members;

α_j is the angle determining the member position when the hydro-cylinder rood moves;

$F_{\text{в.зв}}$ is the force acting on the driven member, i.e. the force at point *B*, point *C* and point *K*, respectively, directed perpendicular to the vector radii *AB*, *BC* and *CK*;

$F_{\text{шт}}$ is the force acting on the hydro-cylinder rod;

G_i is the gravity of the boom turning mechanism members, the stick and the bucket swinging.

2. Results and discussion

Figure 5 shows the performance of the bucket swinging mechanism in the form of the graphs of changing the relative values of the power parameters implemented on the bucket during the working stroke.

The relative values of the power parameters (the forces on the bucket teeth) increase when the hydraulic cylinder rod is extended by about half the working stroke, and then decrease.

So, the operating characteristic of the bucket swinging mechanism under consideration does not provide a correspondence between the values of the power parameters implemented on the bucket and the bucket loading mode, which is characterized by increasing the magnitude of external loads in the course of digging. Therefore, when excavating rock, at the end of the working stroke the hydraulic engine will be overloaded, which can lead to the operation of the safety valve and the working process termination.

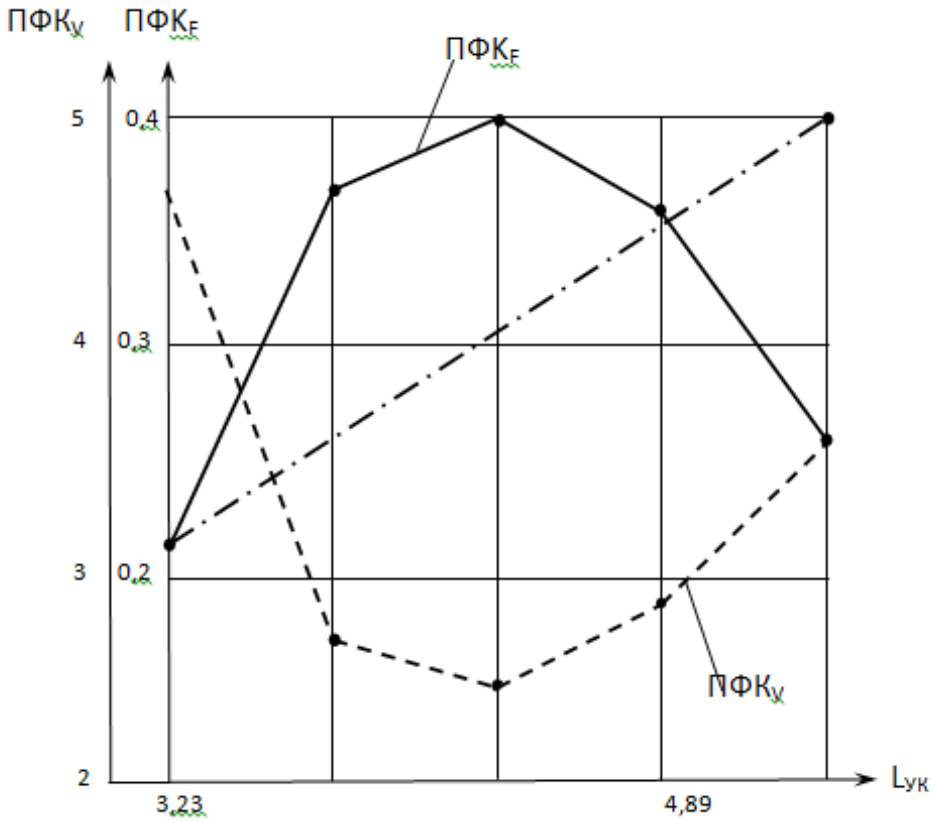

Fig. 5. – Graph of the bucket swinging mechanism transfer function

$ПФК_F$ = *0,21; 0,38; 0,40; 0,36; 0,27*
$ПФК_V$ = *4,8; 2,6; 2,5; 2,75; 3,7.*

The dashed-dotted line shows the rational power transfer function.

Thus, the nominal mode of operation of the hydraulic engine of the bucket swinging mechanism with full use of the rated engine power can be realized with the ideal performance of the bucket swinging mechanism in the form of a monotonically increasing function.

A feature of the loading modes of the main mechanisms is changing both working and reactive loads, and active loads of torque on the driven member (developed by the force on the hydraulic cylinder rod).

The analytical determination of working reactive loads is not possible, since, on the one hand, working and reactive loads depend on the position of the elements of the working equipment in the working area of the excavator when active loads change, and, on the other hand, on the dynamic transfer function and dynamic kinematic properties of lever-hydraulic mechanisms. The solution of such a problem can be performed as a result of numerous calculations that consist in determining both working reactive loads and active loads at off-design points of the working area.

The above algorithm is able to determine the efforts when digging and transporting the bucket, when changing the amount of extension of the hydraulic cylinder rods for turning the elements of the working equipment. The coordinates of the top of the bucket tooth and the forces when digging are displayed in segments on a scale on the sheet, they display the working area of the excavator (Figure 6), the values of the forces on the hydraulic cylinder rods and in the hinges of the working equipment are displayed on diagrams (graphs based on the data of the lower trajectories) (Figure 7).

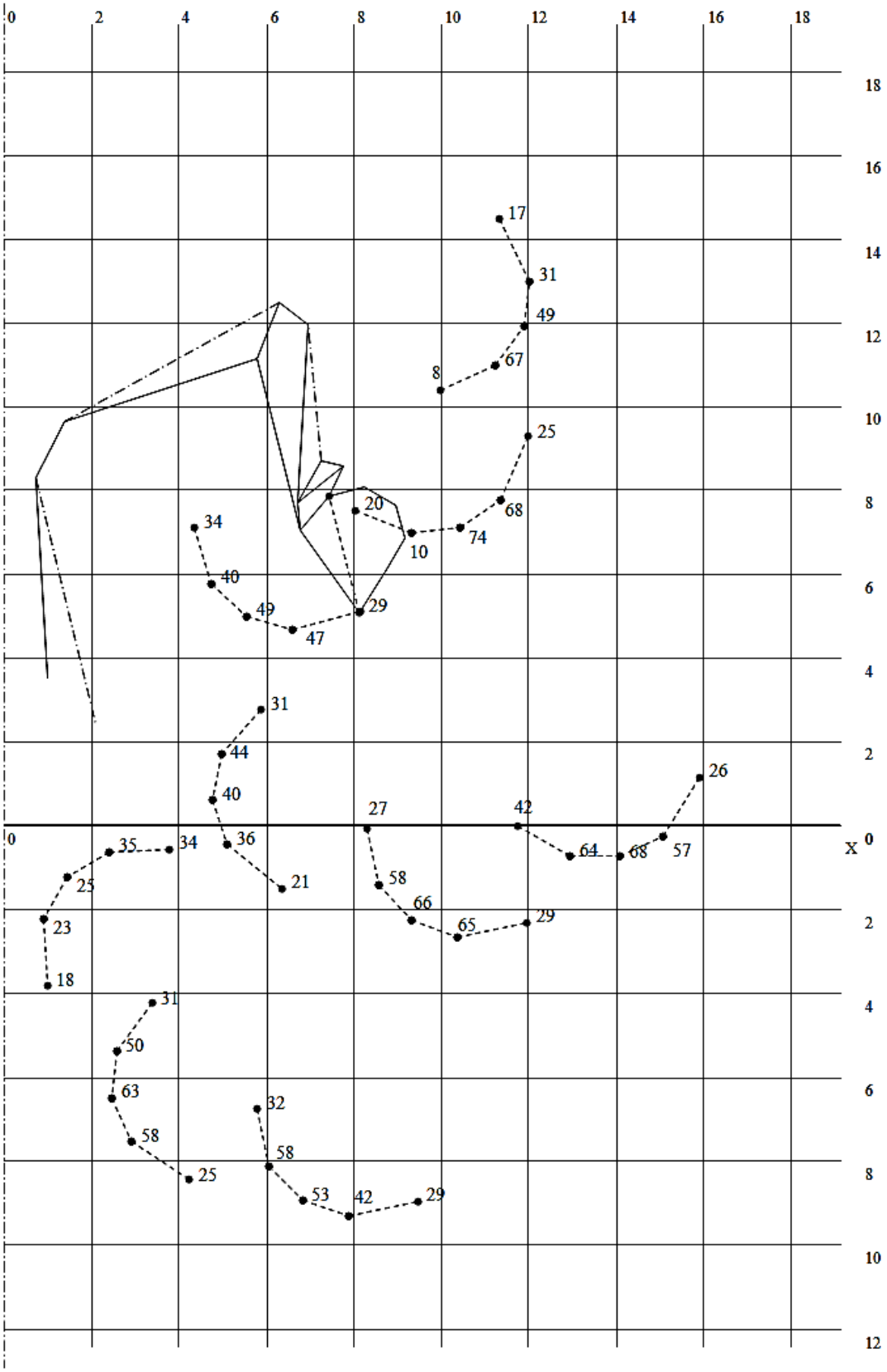

Fig. 6. – The working equipment position and the trajectories of the bucket tooth top

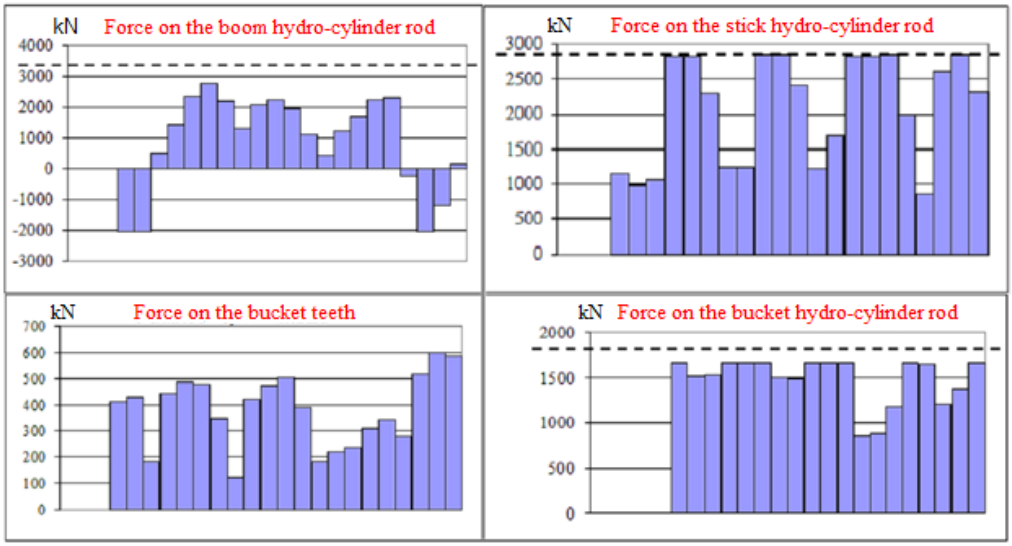

Fig. 7. – Forces on the hydro-cylinder rods of the working equipment

The analysis of the data shows that the possible force on the bucket teeth at almost all points is limited by the pressure in the bucket hydraulic cylinder. The values of forces at the beginning of the digging path by turning the bucket are determined by the leverage of the bucket: *LS* approaches *RS* (Figure 8).

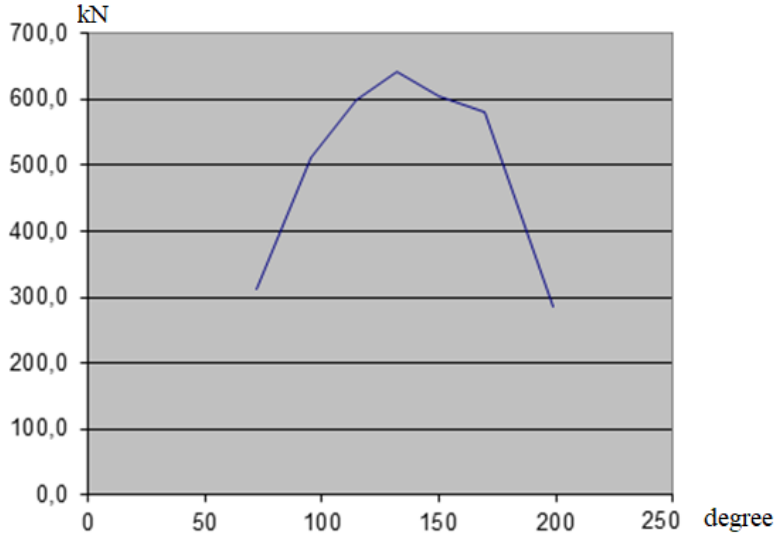

Fig. 8. – Digging force P_{01} dependence on the bucket turning angle

Conclusions

The analysis of the operating characteristics of the working equipment mechanisms will allow assessing the degree of the kinematic schemes of the mechanisms effect on the mechanisms efficiency and in general on the hydraulic excavator.

The synthesis of ideal performance characteristics of working equipment mechanisms will increase the degree of using the rated power of drive engines and ensure ultimately high technical and economic performance of hydraulic excavators.

The developed mathematical description and methodology, the algorithm of which is implemented in the algorithmic language, provides the calculation of digging forces for the entire working area.

The analysis of the research results will allow substantiating the rational design and mode parameters of the working equipment in terms of providing the required technological parameters for working out the face.

References

[1] Borshch-Komponiets L.V. Methods of operational evaluation of open pit hydraulic excavators //Gornaya promyshlennost, No. 1., 1996. - P. 29-37 (in Russian).

[2] Vinitsky K.E. et al. Development of hydraulic excavators of a new generation in the practice of open pit mining //Gornaya promyshlennost. No. 1. - P. 30-36 (in Russian).

[3] Komissarov A.P., Lautenshleiger A.A., Suslov N.M. Evaluation of the energy parameters of the working equipment of hydraulic excavators. Heavy Engineering, No. 8., 1991. - P. 25-29 (in Russian).
[4] Bules P. Operating efficiency of open pit excavators with electromechanical and hydraulic drives of the main mechanisms. //Gornaya promyshlennost, No. 6 (118), 2014. - P. 36-37 (in Russian).
[5] Wisbek Z. et al. On the effectiveness of the use of career hydraulic excavators. *Mining industry*. No. 5, 1998. - P. 25-29.
[6] Dudczak A. Excavators: theory and design. Warsaw: PWN, 2000. – 253 p.
[7] Geu Flores F., Kecskemethy A., Pottker A. (2007). Workspace analysis and maximal force calculation of a face-shovel excavator using kinematical transformers. 12th IFToMM World Congress, Besancon, June 18-21, 2007. – P.6 – 9.
[8] Frimpong S., Hu Y., Chang Z. Perfomance simulation of shovel excavators for earthmoving operations // In Summer in computer simulation conference (SCSC⁄03), 2003. - P. 133-138.
[9] Hall A. Characterizing the operation of a large hydraulic excavator. Master Diss. School of Engineering the University of Queensland, Brisbane, Australia, 2002. - P. 150.
[10] Park B. Development of a virtual reality excavator simulator: a mathematical model of excavator digging and a calculation methodology. PhD Diss. Virginia Polytechnic Institute and State University. Blackburg, Virginia. USA, 2002. - 223 p.
[11] Rath H. Development of Hydraulic for Quarring Applications. Pt. 1. Mine & Quarry, 1987. - P. 26-30.
[12] Komissarov A.P., Shestakov V.S. Simulation model of the functioning of the working equipment of a hydraulic excavator. Mining equipment and electromechanics, No. 8, 2013. - P. 20-24 (in Russian).
[13] Poderni R.Yu. Mechanical equipment of quarries: Textbook for universities. - 8th ed., revised. And extra. - M.: Publishing house "Mining Media Group", 2013. - 594 p. (in Russain).
[14] Komissarov A.P., Lagunova Yu.A., Shestakov V.S. Interrelationships of design and regime parameters of hydraulic excavator working equipment //Mining equipment and electromechanics. No. 11, 2014. - P. 9-14 (in Russian).
[15] Pobegailo P.A. Powerful single-bucket hydraulic excavators. The choice of the main geometric parameters of the working equipment at the early stages of design. - M.: LENAND, 2014. - 296 p. (in Russian).

Information of the authors

Teliman Irina Victorovna, senior lecturer of the department "Technological equipment, mechanical engineering and standardization" Karaganda Technical University
E-mail: ir4ik87_telbez@mail.ru

Malybayev Nurlan Sakenovich, candidate of technical sciences, associate professor of the Department "Technological Equipment, Mechanical Engineering and Standardization" of Karaganda Technical University
E-mail: malybaevnurlansakenovich@mail.ru

Beskorovayny Pavel Gennadievich, senior lecturer of the department "Mechanics" of Karaganda Technical University
E-mail: beskorovayny_p@mail.ru

Ibrayeva Nazira Raissovna, lecturer of the department "Technological equipment, mechanical engineering and standardization" of Karaganda Technical University
E-mail: nazira9407@gmail.com

Komissarov Anatoly Pavlovich, doctor of technical sciences, professor of the department “Hoisting and Transporting Machines and Robots” of Ural State Mining University
E-mail: komissarov_a_p@mail.ru

DOI 10.52209/2706-977X_2022_1_27 **IRSTI 55.53.29** **UDC 621.879.34**

Metal Constructions of Working Equipment of Single-Shovel Hydraulic Excavators: Analysis of Existing Theoretical Approaches to Their Calculation

Pobegailo P.*
Mechanical Engineering Research Institute of the Russian Academy of Sciences (IMASH RAN), Moscow, Russia
*corresponding author

Annotation In this work, its authors present the main results of their analysis of literature on the design and calculation of working equipment (WE) of single-shovel hydraulic excavators (HE). In the process of the review, the studied literature was compared by us with the well-known experimental studies of excavators and with the engineering documentation (ED) known to us.
The present studies have shown that, firstly, there is a great amount of problematic questions that were known a long time ago, but have not been subjected to research, sometimes being solved empirically, but most often being paid little attention. Secondly, in the field of knowledge we are considering in recent years, the Russian science has lost many achievements and was discarded many decades ago. Thirdly, the use of modern technologies is mainly decorative, fake in nature, since the authors of most of these works do not understand what they are doing and even less understand what they have received. Fourth, many foreign works are similar to the Russian ones and cannot be a panacea. Based on the analysis, the authors made an obvious main conclusion: the modern scientifically justified theory of design and calculation of both working equipment and the entire single-shovel hydraulic excavator does not exist in our countries now.

Keywords: hydraulic excavator, working equipment, static loading, method of calculation.

Introduction

The single-shovel hydraulic excavator (HE) is today, in our opinion, the main machine in open mining. Now these machines are widely used around the world (Australia, Canada, China, the Russian Federation, the USA, Sweden, South Africa, South Korea, etc.). At the same time, they face the need to work in hard and very different external environments: "temperatures from -60°C to + 55°C; air humidity up to 95% (and sometimes higher), significant pulse (up to 5g) and vibration loadings (up to 2g) at frequency of 2-6 Hz", etc. [1]. All this creates significant problem for a sustainable, reliable and effective "life" of HE.

On the other hand, the creators of HE are constantly subjected by society and its institutions, which tirelessly form an increasingly rigid frame in the form of conflicting requirements for ensuring the maximum possible productivity (and/or efficiency) while guaranteeing maximum safety (including environmental), which, in particular, is expressed both in intensification of the unit sizes of HE, and in the constant complication of the system, elements and nodes of these machines.

Thus, the modern HE is an already established robotic, manipulative (mechatronic) complex, which will be further complicated in the future. This, in turn, already now poses fundamentally new requirements for the theory of its design, and in particular, for the methods of its calculation.

In some of our works the first steps have been taken to create a fundamentally new methodology for the design of HE in the early stages of its creation. One of the most important stages - after the synthesis of its working equipment (WE), there is the stage of analysis of its static loading which is organically connected to the main design calculations of metal structures (MC).

For this reason, conducting the analysis of the condition of this field of knowledge in the Russian Federation is of great interest, in the republics of the former USSR and in the world with the purpose of further intensifying the processes of creating such machines in the Russian Federation. Moreover, the Russian Federation has adopted a state program for coal mining until 2030, which provides for a significant increase in coal-production (the Program for the Development of the Coal Industry Russia for the period until 2035. Order from June 13, 2020 №1582-r).

At the same time, in this work, first of all, we will focus on the analysis of works related to HE working equipment (WE), touching others only if necessary, since it is the working equipment (WE) that is the first designed subsystem of the machine that determines all its main characteristics, and the requirements for all other subsystems. Fundamentally, it is also for selecting an effective machine operation technology.

Before moving to the main part of this work, we note that this work, as well as the materials of our other works, for example monographs [2,3], are organically interrelated in the framework of the creation of a system of express-diagnostics of quarry excavators, which we are also developing at present.

1. Degree of development of the topic

The following engineers and scientists made a significant contribution to the development of various applied methods for analyzing WE (including MC, and working parts) of SHE (and adjacent machines) (the list is certainly not full): Eisenstat A.R., Agaronik M.Ya., Akinfiev A.A., Yu.D. Afanasyeva, Babushkin A.V., Balovnev V.A., Bashkirov V.A., Belyakov Yu.I., Bondarovich B.A., Brovin V.A., Voloboev V.G., Volodko A.K., Gaitsgori M.M., Gerasimova

T.A., Glezer V.L., Grigoriev A.G., Grigoriev R.S., Goldin Yu.M., Goncharov N.V., Golba A.V., Dyomin A.A., Dzintars U.Ya., Doronin S.V., Elizarova V.B., Zhiveynov N.N. [4], Zaretsky L.B., Zimin A.I., Zlochevsky A.Yu., Ilyin A.E., Isakov V.S., Kabashev R.A., Karasev G.N. [4], Kovalchuk V.A., Koksharov I.I., Kolesnikova S.I., Kondrakhin G.A., Koch P.I., Krivelskaya N.V., Krikun A.V.,Krikun V.Ya, Kozlov M.V., Komissarov A.P. [5], Kondratieva L.Yu., Korolev A.V., Korotny P.V., Kuzmin S.S., Larionov V.P., Lifshits V.L., Lurie G.K., Matyukhin V.I., Mikhailychev S.K., G.D. Moiseyev, Moskvichev V.V., Nabiullin R. [10], Ozol O.G., Pavlov V.P., Panteleenko A.B., Pereponov V.I., Perlov A.S., Pobegailo A.P., Pyndak V.I., Rabatov O.J., Rebeko L.V., Reish A.K., Rudis M.A., Ryakhin V.A., Saidaminov I.A., Svirsky V.A., Semenova N.S., Skobelev L.S., Smolyanitsky E.A., Stebakov I.M., Tymoshenko V.K., Tarassov V.N., Totolin P.E., Fedorov D.I., Khmara L.A., Chaplygin I.A., Chastukhin L.M., Chernov Yu.B., Shamonin A.S., Shilovich V.P., Shipitsyn M.N., Shestakov V.S., Shlykov V.N., Asenov E., Gurko A.G., D.I. Danchev, Krul K., Minin I., Mitrev R., Panov V., Trumper T., Khristov H.P., Sheiretov K.T., Araya H., Avdic H., Bošnjak S.M., Bares J., Beitz W., Brach I., Cannon H., Danko G., Dayawansa P., Ding H., Dudczak A., Elwi A., Enes A.R., Engel S., Imanish E., Inyang H., Jakubczak H., Janssen B., Janosevic D., Frimpong S., Fujita, K., Geu Flores F. [1], Gilbert G., Guiju Z., Hall A., Hiller N., Hoshi A., Hsin-Sheng Lee, Kawabata M., Kecskemethy A. [1], Kemps T., Kim D., Koivo A.J., Lipsett M.G., Maeda G.J., McAree P.R., Miedema S., Nguyen Q.H., Park B., Reece A.R., Rye D.C., Salcudean S.E., Schwappach D., Sing S., Smolnicki T., Tamura K., Tiwari R., Xiao C., Vladeanu A., Walczewski R., Yener M., Yin Y. and other.

The part of the achievements in the USSR was accumulated in calculation documents. Several old books are also known, including the part of the design calculations of certain types of excavators - HE.

Unfortunately, the publication format does not allow you to specify a full list of links - there are about 200 of them. For more detailed information on the topic and the scientific directions related to it, please refer to the foreign reviews and publications of the above authors. We have taken the results of these reviews into account when forming the material presented below.

Our main scientific results in this field are presented in the works [6-8, etc.] and based on this review, which is written without their consideration.

Let us note that this work adds up our other works that have a review nature, (for example 9).

2. Results and discussion

The first works related to the issues we are considering now appeared in the late 50s, early 60s of the last century (and if you look at all single-shovel excavators retrospectively - then they appeared thirty years earlier), and they count at least dozens. Obviously, their "linear" analysis takes more than a dozen pages, which is not suitable for this article. Therefore, now we will present only the main conclusions formulated by us after studying the main works in the scope of works relating to the MC WE HE.

So (let's assume that using the term "domestic" we mean the Russian Federation and Kazakhstan together):

1. From the very beginning of HE creation, the question arose sharply with various calculations of MC. At the same time, the construction mechanics of excavators did not appear, but the methods of general technical disciplines were used (and continue to be used) (as an example we will point to the well-known works by Pankratov S.A. and Ryakhin V.A., it should also be noted about the great contribution of the academician Gudtsov N.T. and Belyaev N.M., as well as Peters E.R. {all for shoveling machine} and Gokhberg M.M. to these issues in the pre-war years (after the war - excavators draglines in collaboration with Vinokursky Kh.A., UZTM) - all this was later largely used for SHE). It should be noted that many of the results of these studies have never been published or summarized;

2. It is essential to note the fact that in the domestic excavation industry there was no transition from the method of calculation by permissible stresses to the method of calculation by limit states (compared to domestic construction, there is a backlog of more than fifty years several works of Lifshits V.L.), published in the second half of the 80s of the last century, did not have time to change the situation and remained, in fact, not completed};

3. In the light of the above-mentioned phenomena about the evolution of SHE, it is obvious that the existing Soviet industry recommendations on the application (for example) materials resistance methods are obsolete (let us note that at the same time almost all the methods implementing them and the programs corresponding to these methods are lost), and the criteria for the mechanics of destruction, unfortunately, have not yet been brought to engineering application (it is difficult to expect rapid positive changes in this issue);

4. Already since the end of the 60s of the last century, the benefits of using various numerical methods and computers in the synthesis and analysis of various MC have become obvious. Now the use of such methods is supposed to be obligatory in a certain sense and, in fact, routine;

5. The main problem of all studies and calculations related to the assessment (for example) of a stress-strain state (SSS) (when calculating for static strength) and the applying (for example) of the finite element method (FEM), is associated with a reasonable choice of the calculation scheme. Most of the works known to us, especially modern domestic ones (as well as those performed in some countries to the south of the Russian Federation and Kazakhstan), do not pay any attention to this, which significantly limits the possibility of applying the results presented there;

6. In our opinion, a reasonable choice of the calculation scheme should include the following main stages: determining the maximum external loading and selecting the scheme (type and character) of its application to the machine (so-called "loading scheme"); selection of the scheme of crawler attachment support, if the decision to fully analyze the machine is made (possibly taking into account the elasticity of the soil both under the crawler and during the interaction of the shovel with the rock); selection of a numerical method and, possibly, its variety within the

framework of the problem (it is possible that in some problems it is better to apply the boundary element method rather than FEM); selecting a program implementing the selected numerical method; selecting a valid finite element type (or types for their combined use) and finite element mesh density; selection of attachment scheme and boundary conditions of contact surfaces, etc. The most important step is the analysis of the results; The task of estimating the external load of HE is complicated by the fact that its connection with the extreme values of SSS components in various elements of WE is ambiguous, which leads to a significant increase in the volume of calculations. By the way let us note that the issue of the impact of wear on the loading of HE is completely insufficiently investigated, which is important to keep in mind when creating the modern theory of calculating and designing these machines;

7. In modern domestic design activity there is no binding of MC calculations to the set of design procedures (in fact, there are no these procedures), and as a result, there is no set of different physical and mathematical models suitable for application at one stage or another stage of the design (the application of both expensive imported computer programs and the replication of fashion passages about CAE/CAD/CAM etc. "digital economy" is not a significant advance in the construction of HE design methodology, the application of such products plays a brake role more and leads to a reduction in the number of designers whereas their number should be increased).

At the same time, these required models should be as simple as possible and give satisfactory results for design.

8. In addition to the general requirements, the above models applied in solving the tasks of synthesis and analysis of HE WE should have: a) interaction with technical economic calculations TEC (actually there should be the necessary models for TEC); b) complete and consistent classification of kinds and types of loads and impacts (especially in the conditions of mutual influence of machine elements on each other); c) clearly formulated and reasonably resolved problem of controlling the state of SSS MC WE HE (and further the whole machine); d) possibility of changing the design schemes of WE and HE to take into account the assembly - disassembly and transportation of HE to its place of operation;

9. We have not found works in which the question of whether it is permissible to consider WE elements separately (both the base machine and among each other) was studied in detail. The same touches upon other subsystem of excavators (as far as we understand the Japanese consider the entire cars).

Let us note that when regarding WE elements and the whole machine in the complex, it is necessary to take into account: a) the fact that part of HE MC elements is loaded with a weight more than the located constructions {this has never been taken into account before, even during natural full-scale experiments}; b) studs are applied as joints in the part of HE MC. Today there is no understanding of how they operate under conditions of both motion and excavation; c) there is no methodology for calculating support-turning devices (STD) in our countries at the modern level and taking into account the specifics of HE. It is not completely clear how loadings are transmitted lower by means of STD and what idealizations are allowed. This is accompanied by problems with the ability to perform calculations of the elements of STD - for example, rollers (an important role in the conglomerate of these problems is played by the choice of the type of frame for STD - it has long been proved that the conical frame has a number of significant advantages (in the works by Ryakhin V.A. and Totolin P.E. in the 80s of the last century) {and later in the works by Doronin S.V.}, however, in real practice, such designs were not used **(**it is only known that they wanted to be used at the Krasnoyarsk Heavy Engineering Plant, but without result)); d) taking into account the elasticity of the soil under HE caterpillars, it is possible to apply a large range of models of soils known from mechanics. (Here it is useful to recall works of a similar nature for excavators of draglines performed at the V.V. Kuibyshev MECI, at the UHEP and SMI named after V.V. Vakhrushev State; there were also works for rotary complexes, caterpillar cranes, etc.) {the issue of dynamic stability of SHE is significant as well, which today is not fully considered and not taken into account in the design}. It is not clear which models are more rational and not clear whether they necessarily require the boundary element method or they can be calculated by conventional MFE; e) for many calculations of newly created HE, the relevant question of where the loading of the machine is greater - when moving or excavating (it is obvious that there is no universal answer here). In addition to the main shovel, the application of other working equipment requires special studies from this perspective (the same touches upon the standard types of WE); e) modern HE are often used in unusual (not habitual) way - from digging by the return shovel higher than the level of its parking and up to various "dances" with the support on the shovel, etc. All these modes are not investigated and, as a result aren't considered while designing (in this case, we would recommend prohibiting such modes, and in case of violation the ban, to abolish the guarantee on the excavator). Taking into account these modes requires special studies (especially in terms of the impact on the fatigue life of HE);

10. It should be noted that when estimating STD WE HE the deformations are often forgotten, which seems unacceptable. In addition, the methodology for analyzing STD for SHE shovels in our country has not been practically developed (in fact, the theory of calculating shovels is at the level of the mid-60s of the last century and, moreover, in an extremely disparate form). We also note that sometimes in some HE designs (for example, a rotary platform) there may be the so-called "shaking" effect {An excavator is loaded cyclically. While repeated loadings, residual deformations can grow and reach a significant value. As the loading increases, the plastic deformations increase. With a certain load value, the bearing capacity of the construction becomes exhausted. This condition is called the loss of stability of the second type} - this issue for HE has not been studied at all (in the USSR it was taken into account only in the design of ED for the calculation and design of MC car cranes).

11. Practically we do not know useful works, which would take into account the features of contact interaction in hinges (there are also very few theoretical works known to us and they are very outdated). A well-known academic interest is also the accounting of roughness and the use of new, for example, composite, materials. This issue should be

at the centre of HE research in the present century (this is also important because of the problem of wear and sticking of soil);

12. A separate subclass of works form the works on the convergence of calculations when applying MFE to practical tasks (Doronin S.V. with colleagues). It is necessary to intensify these studies and ensure their implementation into design practice;

13. The only powerful scientific school for the practical application of the MFE and the theoretical study of all the main issues has been preserved in Krasnoyarsk (SDTB "Science" FRC «KSC of the SB of the RAS»). It would be good if they were involved in work at domestic plants in the development of both calculation documents and standard design procedures (the introduction of the theoretically so-called "probabilistic risk analysis of structures", which would contribute to the emergence of reliability calculations in the design practice, that had been long forgotten, taking into account the important provisions of the ED created for road construction machines in the USSR by the efforts of Khazov B.F. and his employees). All this could help to reduce our backlog from the Western countries in the creation of excavators for the conditions of space (today it is more than 30 years);

14. There is no work justifying how (and if it is necessary) to model hydraulic cylinders when consideration WE MC, while they are elastic elements that affect the dynamics of the whole WE (and the whole machine);

15. In the well-known literature on excavators, there is no approach to taking into account the features of WE welds;

16. Mainly MFE is used for STD analysis and, as a result, for static strength calculations. This is certainly not enough;

17. It is necessary to resume the work on the creation of statistical dynamics of single-shovel excavators (based on the work of B.P. Bagin, the works of KHADI and the results obtained at the scientific school of Fyodorov D.I.

Conclusions

In the conclusion of this work, the following can be said:

- in our country there is no methodology for designing WE HE that fully takes into account modern ideas about the processes of degradation of construction materials, the criterion base of design calculations is limited, and the MFE is not applied sufficiently substantiated;
- despite the frequent use of MFE, the design schemes for these studies are not optimal;
- The definition of external loading (even in static tasks) is not sufficiently studied;
- no exact answer was received on the admissibility of separate calculation of the elements of WE and HE, although they are considered in this way much more often (apparently to save time). In addition, it is not clear whether it is permissible not to take into account hydraulic cylinders and contact interaction in hinges;
- the process of designing WE and HE in our country is poorly automated, and in the methodological meaning is not developed, and not reflected;
- in our country, there are practically no work related to the application of MFE to the problems of cutting and drawing soil (here our lag seems to be at least thirty years);
- for optimal justification of design schemes it is necessary to return to natural full-scale experiments (with special attention to hydraulic cylinders and control of their drive schemes);
- it seems promising to organize a scientific search both in terms of the use of new materials and new modeling methods for the industry, for example, using neural networks [11];
- it is necessary to integrate detailed dynamics analysis into the design procedures, for which purpose the necessary physical models and their mathematical description should be developed.

Thus, the current state of the domestic field of knowledge about the implementation and content of the complex of design calculations of both MC WE and the entire SHE must be recognized as not satisfactory (the theories meeting the requirements of our time have not been developed).

References

[1] Geu Flores F., Kecskemethy A., Pottker A. Workspace analysis and maximal force calculation of a face-shovel excavator using kinematical transformers //12th IFToMM World Congress, Besancon, June 18 – 21, 2007. – P. 6 – 8.

[2] Pobegailo P. A. Powerful single-shovel hydraulic excavators: working equipment design methodology (in the early stages of design). - M.: SvR-ARGUS, 2017. - 210 p.

[3] Pobegailo P. A. Powerful single-shovel hydraulic excavators: selection of basic geometrical parameters of working equipment at the early stages of design. - M.: LENAND, 2014. - 296 p.

[4] Zhiveynov N. N., Karasev G. N., Tsvey I. Yu. Construction mechanics and metal structures of construction and road machines. - M.: Engineering, 1988. - 280 p.

[5] Komissarov A.P., Shestakov V.S. Simulation model of functioning of working equipment of hydraulic excavator //Mining equipment and electromechanics, № 8, 2013. – P. 20 – 24.

[6] Pobegailo P. A. Some geometric properties of the working equipment of single-shovel hydraulic excavators: Mining Information and Analytical Bulletin (scientific and technical journal) Individual articles (special issue), № 1, 2014. - 28 p.

[7] Pobegailo P. A. Solution of direct positional problem for single-shovel hydraulic excavators //Mining information and analytical bulletin, № 12, 2014. – P. 193 – 197.

[8] Pobegailo P. A. Mathematical model for determining the loading of a single-shovel hydraulic excavator of reverse digging //Interstroymech. - 2002: Materials of the international scientific conference/MSTU, Mogilev, 2002. - P. 179 – 181.

[9] Pobegailo P. A., Kritsky D. Yu. Sticking of soil to metal constructions of excavators: about the modern state of the problem //Mining information and analytical bulletin, № 50, 2018. – P. 204 - 215 DOI 10.25018/0236-1493-2018-12-50-204-215

[10] Nabiullin R., Teliman I., Khoroshavin S. The interaction of the main actuators of hydraulic excavators //E3S Web Conf, Volume 177, 2020, XVIII Scientific Forum "Ural Mining Decade" (UMD 2020) DOI https://doi.org/10.1051/e3sconf/202017703013
[11] Lagunova Yu., Shestakov V., Ibraeva N. The study of the movement of a piece on the camera crushing in network type bases as applied to the workflow of the FCC» //E3S Web Conf., Volume 177, 2020, XVIII Scientific Forum "Ural Mining Decade", UMD 2020 DOI https://doi.org/10.1051/e3sconf/202017703011

Information of the authors

Pobegailo Petr Alexeevich, candidate of technical sciences, associate professor of Mechanical Engineering Research Institute of the Russian Academy of Sciences
E-mail: petrp214@yandex.ru

DOI 10.52209/2706-977X_2022_1_32 **IRSTI 55.53.09** **UDC 669.295:539.214**

High-Entropy Strengthening Coatings on Rolling Stock Locomotive Parts

Portnov V.S. [1], YurovV.M. [2], Makhanov K.M. [2],
MausymbaevaA.D.[1*], Madisheva R.K.[1], Isatayeva F.M.[1]
[1]Karaganda Technical University, Karaganda, Kazakhstan
[2]Karaganda University E.A. Buketov, Karaganda, Kazakhstan
*corresponding authors

Abstract. Our studies have shown that parts of locomotives of rolling stock coated with FeCrNiTiZrAl microhardness increases by about 1.6 times, wear resistance increases by 7.5 times; the coefficient of friction is reduced by almost 10 times, and the resource of parts is almost three times, which is very significant economically.

Key words: hardening, microhardness, wear resistance, coefficient of friction, service life.

Introduction

Locomotives provide the movement of trains on the railways [1, 2]. Creating a driving force (traction force) F when interacting with the rails and moving the train by a distance S due to this force, the locomotive performs useful mechanical work A, equal, since the direction of the force action coincides with the direction of movement, to the product of these values.

The rolling stock is used for the transportation of goods and passengers (Figure 1).

Fig. 1 - Rolling stock

The rolling stock consists of a driving locomotive and wagons attached to it, which it pulls along with it. Depending on the source of energy and mechanisms for converting it into mechanical work, the rolling stock is divided into autonomous and non-autonomous. Autonomous operates on its own reserves of energy sources. The non-autonomous rolling stock receives electricity by wires from an external source. The most important for railway transport methods of restoration and strengthening of parts, depending on the thickness of the applied layer, can be divided into three groups [3].

Small thicknesses:
1) Electroplated coatings;
2) Vacuum spraying;
3) Electrospark alloying;
4) Gas cladding and spraying;
5) Electrometallization;
6) Plasma surfacing and spraying.

Medium thicknesses:
1) Electrical contact surfacing and cladding;
2) Vibration arc surfacing;
3) HDTV surfacing;
4) Cladding in CO_2 environment;
5) Flux-cored wire surfacing;
6) Argon arc surfacing.

Large thicknesses:
1) Submerged arc surfacing with solid wire;
2) Cladding under ceramic flux;
3) Welding with an electrode strip;
4) Electroslag surfacing.

In this article, continuing work [4], we will discuss reinforcing high-entropy coatings on parts of rolling stock locomotives.

1. Experimental technique

To prepare the FeCrNiTiZrCu target, micropowders of the corresponding metals were taken and mixed in equiatomic proportions. Then, two magnetron targets were made according to the technique described in [5] (Figure 2). One target is made by melting a mixture of micropowders in a vacuum oven at a temperature of 1200 °C (Figure 2a), and the second target is made of "tablets" 5 mm in diameter on a steel substrate by annealing these tablets in a vacuum oven at a temperature of 1200 °C (Figure 2b). For coating, the following parts were provided on steel type 12X13 of rolling stock locomotives (Figure 3a). A vacuum setup with two magnetrons was used for coating (Figure 3b). The cylinder is designed to move the working body from one position to another. The pneumatic cylinder includes a cylinder body, a pressureless head, a hollow piston rod, a piston head and a push rod.

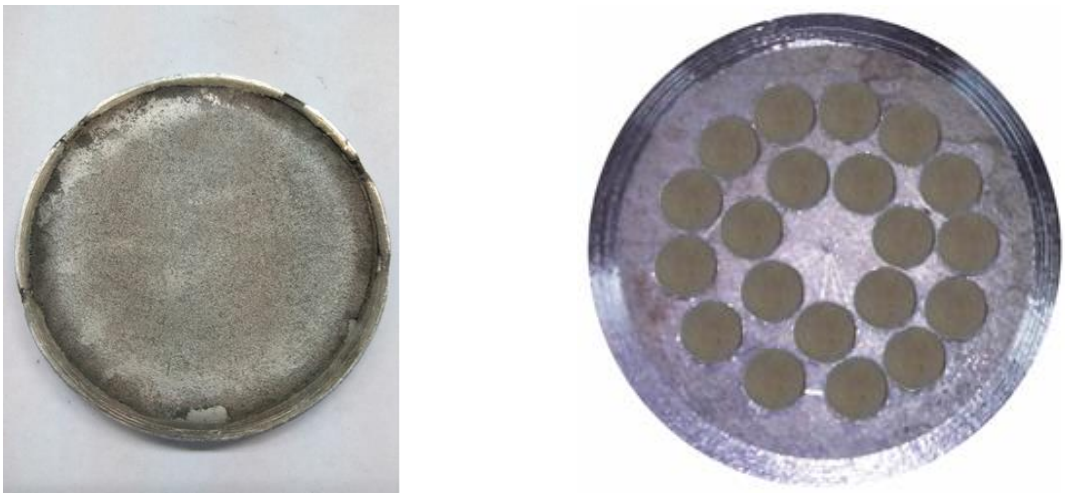

a) b)

Fig. 2 - Targets for coating: cast target (a), tablet target (b) [5]

a) b)

Fig. 3 - Connecting pin of the drive disk on steel 12X13 (a), sputtering unit with two magnetrons (b)

The cylinder body has a mounting flange and an inlet. The unpressurized head has a mounting flange. The hollow piston rod has an open end and a closed end. The piston head is attached to the hollow piston rod and forms the closed end of the hollow piston rod. The pusher has an insertable end inserted inside the hollow piston rod and a connecting end. The unpressurized head has a hollow rod guide and a hollow rod seal, and the piston head has a piston guide and a piston seal. Both the hollow rod guide and the hollow rod seal are slidably engaged with the hollow piston rod. Both the piston guide and the piston seal are slidably engaged with the cylinder body.

Coating FeCrNiTiZrCu for the first hour on the samples of the connecting pin with two targets with two-row tablets using a dual magnetron power supply with other parameters is performed as follows (Figure 3b):

- the prepared samples are installed in the chamber of the NNV 6.6-I1 setup with the help of the equipment on the satellite of the rotating table;
- the diffusion pump is heated, the chamber is heated (30 min);
- forevacuum pumping is carried out to a pressure of 1 Pa (15 min).
- the heating of the chamber is turned off;
- further evacuation of the chamber is carried out by a high-vacuum diffusion pump up to a pressure of $5 * 10^{-3}$ Pa (30 min);

- then gas (argon) is supplied to the chamber and the pressure in the chamber is maintained at $2*10^{-1}$ Pa using the "BUEN" solenoid valve control unit;
- the table rotation drive is switched on and the rotation speed is set to 5 rpm;
- the plasma source with a hot cathode "PINK" is switched on, the glow current is set to 130 A, the ion current is 5 A, focusing is 0.7 A;
- the block of reference voltage is switched on and a bias voltage from 300 V to 1000 V is applied to the part as the samples are cleaned and micro arcs appear (15-20 min);
- after cleaning the samples, the reference voltage is reduced to 200 V;
- "PINK" is turned off;
- the dual power supply unit of magnetrons turns on. The parameters are set P = 1.7 kW, U = 700 V, I = 2.45 A (1 h);
- after the end of the spraying, the dual power supply unit of the magnetrons is switched off;
- then the gas supply stops, the supply of the reference voltage stops, the rotation of the table is turned off;
- the heating of the diffusion pump is turned off, the heating of the chamber is turned on;
- let the samples cool down and, when the chamber heats up, let the air in
using the valve and take out the samples (30 min).

Figure 4a shows parts with FeCrNiTiZrCu coating on 12X13 steel, and figure 4b shows parts with TiN coating.

Electron microscopic examination was carried out on a scanning electron microscope MIRA 3 from TESCAN. The studies were carried out at an accelerating voltage of 20 kV and a working distance of about 15 mm. For each sample, four images were taken from four points on the surface at different magnifications: 245x, 1060x, 4500x, and 14600x (Figure 5a). Using an electron microscope, the chemical composition was determined by the XPS method (Figure 5b, Table 1).

a) b)

Fig. 4 - Details of locomotives coated with FeCrNiTiZrCu (a) and coated with TiN (b)

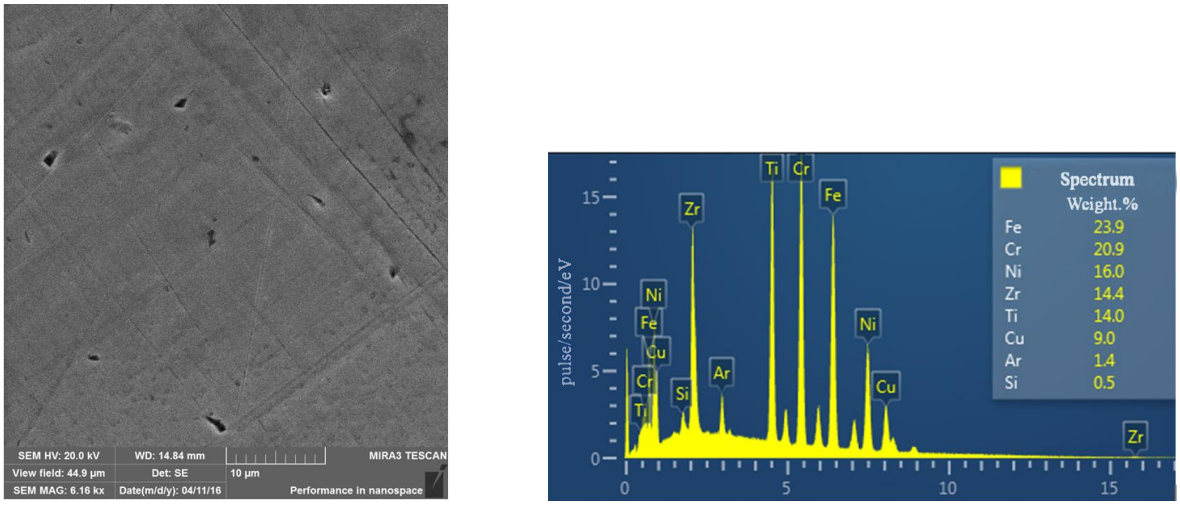

a) b)

Fig. 5 - SEM - image of the coating at a resolution of 10 nm (a), XPS FeCrNiTiZrCu in argon (b)

The resulting alloy mainly consists of a simple bcc solid solution and belongs to HEAs, and the total number of phases is much lower than the maximum equilibrium amount allowed by the Gibbs phase rule.

Table 1. Quantitative chemical composition of FeCrNiTiZrCu, at.%

Element	Fe	Cr	Ni	Ti	Zr	Cu
in argon	23,9	20,9	16,0	14,0	14,4	9,0

We used a HVS-1000A microhardness tester (Figure 6a). It can also be used to study the structure of metallic materials and to determine the distribution of cementite over the surface and experiments with determining the hardness according to the Knoop method (1 GPa = 92.6 HV). The results of measurements of FeCrNiTiZrCu coatings are given in Table 2.

Table 2. Microhardness of the FeCrNiTiZrCu coating in argon

Microhardness	1	2	3	4	5	6	7	8	average
HV 0,05 = 0,49N	742,9	722,8	777,2	729,3	722,9	744,7	757,3	733,1	740,0

The microhardness of our FeCrNiTiZrCu coating is not inferior to high-entropy equiatomic alloys and is significantly higher than the microhardness of the coating of stainless steels. The general scheme of the installation for determining the friction coefficients k_{fr} is shown in Figure 6b [6] and includes: 1 - known clamping weight, 2 - sample, 3 - sliding surface, 4 - measuring table, 5 - force transducer, 6 - electronics unit and drive. The measurement results are shown in Table 3.

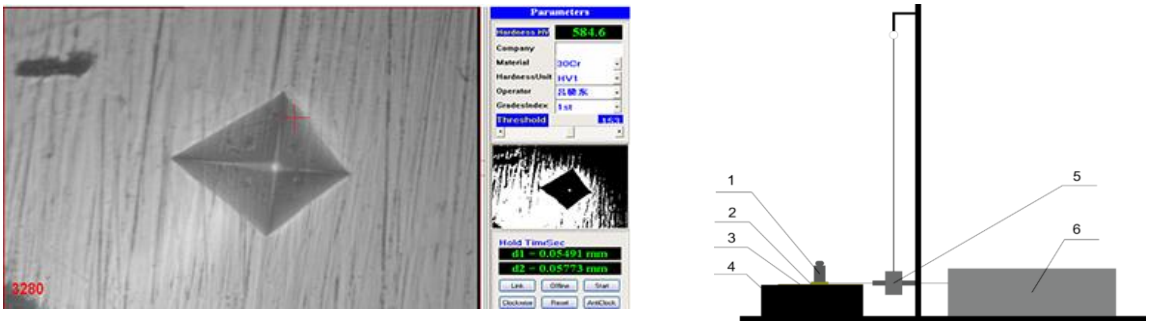

a) b)

Fig. 6 - Microhardness tester HVC-1000A (a) and installation diagram for determining the friction coefficients k_{fr} (b) [6]

Table 3. Coefficient of friction of the FeCrNiTiZrCu coating

Friction coefficient	1	2	3	4	5	6	7	8	average
k_{fr}	0.045	0.052	0.067	0.065	0.061	0.062	0.058	0.055	0.06

To determine the specific surface energy (surface tension) σ, we used the technique described by us in [7]. The first method provides for the measurement of surface tension by determining the dependence of the microhardness on the thickness of the deposited coating. The dependence of the microhardness of the deposited coating on its thickness is described by the formula:

$$\mu = \mu_0 \cdot (1 - d/h), \quad (1)$$

where μ is the microhardness of the deposited coating;

μ_0 is "thick" sample;

h is the thickness of the deposited coating.

The parameter d is related to the surface tension σ by the formula:

$$d = 2\sigma\upsilon / RT, \quad (2)$$

where σ is the surface tension of a massive sample;

υ is the volume of one mole;
R is the gas constant;
T is the temperature.

As an example, consider the determination of the surface tension of the FeCrNiTiZrCu coating on steel 12X13. The results are shown in Figure 7. In the coordinates $\mu/\mu_0 \sim 1/h$, the experimental curve is straightened in accordance with formula (2), giving the value h = 1.3 μm. For the FeCrNiTiZrCu coating, the surface tension obtained is σ = 1.409 J/m^2 (Table 4). This value confirms the wear resistance of the FeCrNiTiZrCu coating on steel 12X13.

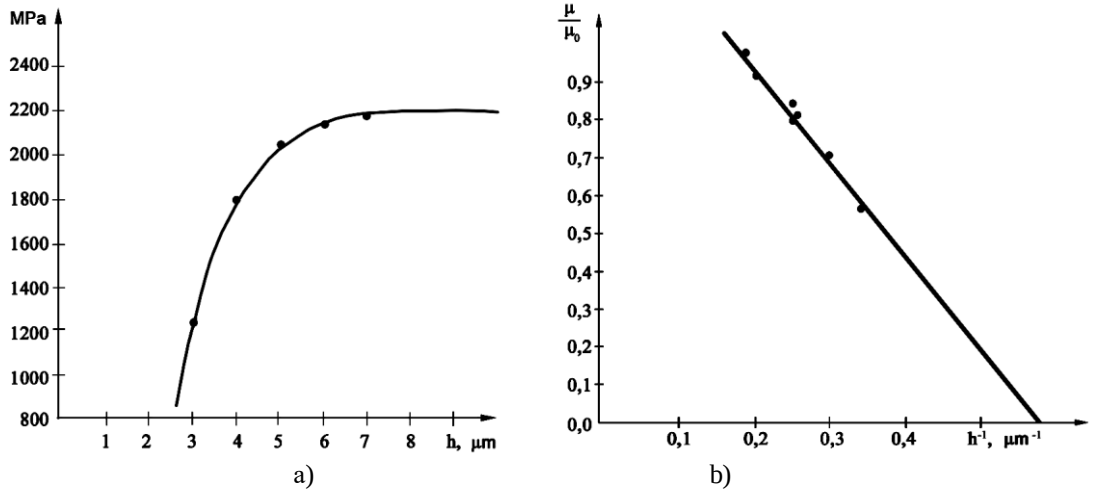

Fig. 7 - Dependence of microhardness on the thickness (a) and inverse thickness (b) of the FeCrNiTiZrCu coating on steel 12X13

Table 4. Surface tension of FeCrNiTiZrCu coating

Superficial tension	1	2	3	4	5	6	7	8	average
σ, J/m^2	1.410	1.391	1.412	1.403	1.405	1.408	1.416	1.417	1,409

2. Results and discussion

Let's compare the hardness of stainless steels [8] with the hardness of high-entropy coatings from Table 2.

The hardness of most stainless steels (especially locomotive parts) is 2-3 times less than high-entropy coatings, which shows the prospect of their use as parts of various industrial structures. Let us compare the friction coefficients k_{fr} of common metals with Table 3.

Table 5. Hardness of stainless steels [8]

Steel	μ, HV	Steel	μ, HV
12X13	121-187	08X17T	372
40X13	143-229	10X17H13M2T	200
08X18H10	170	12X18H10T	179

Table 6. Coefficients of dry friction for homogeneous and dissimilar pairs of the most common metals [9]

Metal	k_{fr}	Metal	k_{fr}
Steel-Steel	0,8	Cr-Cr	0,4
Fe-Fe	1,0	Mg-Mg	0,6
Cd-Cd	0,5	Ni-Ni	0,7
Al-Steel	0,61	Cu- Steel	0,53
Brass-Steel	0,35	Ni- Steel	0,64
Cd-Cr	0,41	WC-Cu	0,35

The dry friction coefficients k_{fr} for homogeneous metal pairs are significantly higher than the dry friction coefficients for dissimilar metal pairs, but still lie in the range 0.35-0.60, which is an order of magnitude higher than the

dry friction coefficients k_{fr} of high-entropy coatings. The latter have dry friction coefficients in the region of 0.06 (Table 3), which exceeds the dry friction coefficients, for example, based on sulfonic acid salts. Such a difference in the coefficients of friction k_{fr} for high-entropy coatings is due to their nanostructural feature and the manifestation of the size dependence of their properties. However, nanostructured TiN coatings have dry friction coefficients of 0.40 [10]. This means that for high-entropy coatings consisting of 5-6 metals, the friction mechanism is somewhat different than the dry friction coefficients k_{fr} for homogeneous and dissimilar pairs of the most common metals. The five theories that exist at present and explain the processes occurring during friction do not contain the size dependences characteristic of nanostructures.

In [6], within the framework of the thermodynamic approach for the dry friction coefficient, we obtained the following formula:

$$k_{fi} = \tilde{N} \cdot \dot{O} \cdot \frac{\sigma \cdot S}{\Delta G^0} \cdot \overline{N}, \quad (3)$$

where σ is the specific surface energy of the material;

S is the contact area;

$\dot{O}$ is the temperature,

ΔG^0 is the Gibbs energy;

$\widetilde{N}$ is the average number of elementary fracture carriers (proportional to the number of defects),

C is a constant.

But according to the molecular-kinetic theory, the friction force $F \sim k_{fi}$ is equal to:

$$F = \int \sigma dL \approx \sigma \cdot L, \quad (4)$$

where σ is the surface energy (table 4);

L is the length of the traveled path.

Equation (3) shows that the coefficient of friction is proportional and increases with increasing surface energy according to (4), that is, the value of σ from Table 4 should lead to an increase in the coefficient of friction. But the opposite picture is observed experimentally, the friction coefficient decreases, which contradicts the molecular kinetic theory, but becomes explainable from the point of view of our formula (3), which contains the Gibbs formula in the denominators and significantly decreases for a high-entropy alloy due to an increase in its entropy. Since tribological properties play an essential role in technology, high-entropy alloys and coatings will take a worthy place among structural materials.

The studies carried out above by us have shown that parts of locomotives of rolling stock coated with FeCrNiTiZrAl microhardness increases by about 1.6 times, wear resistance increases by 7.5 times; the coefficient of friction decreases almost 10 times, and the resource of parts is almost three times, which is very significant economically.

Studies (Table 4) have shown that the maximum surface energy σ is achieved in the [111] plane. Metals with a face-centered cubic (fcc) lattice are deformed along close-packed octahedral [111] planes in close-packed <110> directions. Since the work on destruction of the coating is equal to A = σ S, where S is the area of the coating, a significant increase in surface energy leads to an increase in the resource of parts of locomotives of rolling stock with a high-entropy coating FeCrNiTiZrAl three times.

Conclusions

The application of the FeCrNiTiZrCu coating on the connecting pin samples with two targets with double-row tablets using a dual magnetron power supply led to the following results:

- the microhardness of our FeCrNiTiZrCu coating is equal to 740 HV and is not inferior to high-entropy equiatomic alloys, but much higher than the microhardness of the coating of stainless steels;
- the dry friction coefficients of the FeCrNiTiZrCu coating are in the region of 0.06, which exceeds the dry friction coefficients of conventional metals:
- a significant increase in surface energy leads to a threefold increase in the service life of rolling stock locomotive parts with a high-entropy FeCrNiTiZrAl coating.

Acknowledgments

The work was carried out under the program of the Ministry of Education and Science of the Republic of Kazakhstan Grant No. 0118RK000063.

References

[1] Volodin A.I., Zyubanov V.Z., Kuzmich V.D. and other. Locomotive power plants. - M.: IPK "Zheldorizdat", 2002. - 718 p.

[2] Shapshal A.S., Bogoslavsky A.E., Grigoryants M.K. and others. Locomotives. - FGBOU VPO RGUPS. - Rostov n/a, 2015. - 118 p.

[3] Lobanov M.L., Kardonina N.I., Rossina N.G., Yurovskikh A.S. Protective coatings. - Yekaterinburg: Ural Publishing House. University, 2014. - 200 p.
[4] Portnov V.S., Yurov V.M., Makhanov K.M., Amangeldikyzy A., Kopobayeva A.N. Nitrogening Hammers of the Grain Crusher of the Aknar Poultry Factory // Material and Mechanical Engineering Technology, №1, 2021. – P. 9-13.
[5] Yurov V.M., Guchenko S.A., Tvardovsky A.N. Two targets for magnetron deposition of high-entropy coatings // Trends in the development of science and education, 2020, No. 60 (1). - P. 28-34.
[6] Yurov V.M., Guchenko S.A. Determination of friction of dissimilar pairs of tribo-conjugation // School of Science, 2020, no. 1(26). - P. 5-8.
[7] Yurov V.M., Laurinas V.Ch., Guchenko S.A., Zavatskaya O.N. Surface tension of hardening coatings // Strengthening technologies and coatings, 2014, No. 1. - P. 33-36.
[8] Povolotskiy D.Ya., Gudim Yu.A. Stainless steel production. - Chelyabinsk: SUSU Publishing House, 1998. - 236 p.
[9] Kragelsky I.V., Vinogradova I.E. Coefficients of friction. - M.: Mashgiz, 1962 - 220 p.
[10] Pogrebnyak A.D., Bagdasaryan A.A. Pink A.V., Dyadyura K.A. Multicomponent nanocomposite coatings with adaptive behavior in surface engineering // Uspekhi fizicheskikh nauk, 2017, Vol. 187, no. 6. - P. 629-652.

Information of the authors

Portnov Vassily Sergeevich, doctor of technical sciences, professor of the department “Geology and Exploration of Mineral Deposits” of Karaganda Technical University
E-mail: vs_portnov@mail.ru

Yurov Viktor Mikhailovich., candidate of phys.-math. sciences, associate professor of Karaganda University E.A.Buketov
E-mail: exciton@list.ru

Makhanov Kanat Matovich, candidate of phys.-mat. sciences, associate professor candidate, associate professor of Karaganda University EA. Buketov
E-mail: makhanov_kanat@mail.ru

Mausymbaeva Aliya Dumanovna, PhD, acting associate professor of the department “Geology and Exploration of Mineral Deposits” of Karaganda Technical University
E-mail: aliya_maussym@mail.ru

Madisheva Rima Kopsbosynkyzy, PhD, senior teacher of the department “Geology and Exploration of Mineral Deposits” of Karaganda Technical University
E-mail: rimma_kz@mail.ru

Isatayeva Farida Muratovna, PhD, acting associate professor of the department “Geology and Exploration of Mineral Deposits” of Karaganda Technical University
E-mail: adambekova_farid@mail.ru

DOI 10.52209/2706-977X_2022_1_39 IRSTI 53.49.15 UDC 669.1.017:669.018.44

Research of Exploitation of High Temperature GX40NiCrNb 45-35 Alloy

Lukašius D., Buzaitis K., Černašėjus O.*, Žlioba K.
Vilnius Gediminas technical university, Vilnius, Lithuania
*corresponding author

Abstract: In the paper, the properties and the structure of high temperature nickel-chromium alloy is discussed upon. The principal applications of the alloy are convection coil pipes and tubes sheets for furnaces. This alloy is considered one of the most important in the oilfield. Alteration of the alloy microstructure and conditions of the equipment exploitation are the principal factors that may cause a reduction of its operational life and destruction of the equipment. Hardness and microhardness tests of nickel-chromium alloy after 10 years of its exploitation as well as investigation of its microstructure and chemical composition had been arranged.

Keywords: nickel-chromium alloy; high temperature alloy; microstructure

Introduction

Heatproof nickel-chromium alloys are widely used in petrochemical industry where the industrial equipment operates under extreme conditions. The used alloys enable improving the quality of the equipment and extending its service life; in addition, they reduce production costs. The principal applications of the said alloys include convection coil tubes sheets, suspensions and supports for furnaces. The said alloys are considered the most important alloys in petrochemical industry. Alteration of the alloy microstructure and the conditions of the equipment exploitation are the principal factors that may cause a reduction of its operational life and destruction of the equipment. Usually, a damage of equipment mechanisms is caused by metal fatigue, corrosion cracking and splitting [1, 2].

For alloys applicable in chemical industry, two requirements are of the highest importance; they include corrosion resistance and thermal resistance. Austenite alloys, such as HK40 (Cr25Ni20) and HP40 (Cr25Ni35), were traditionally used over the course of decades, because they are resistant to creeping process and their corrosion resistance is good at the working temperature. However, the requirement related to increased productivity of manufacturing (upon increasing the material exploitation temperature over 1000 °C) and reduction of operating costs tighten up the equipment exploitation conditions in a majority of industrial sectors. The continuous improvement of pyrolysis technologies in furnaces where thermal effect in the heating sections achieves 70–87 kW/m2 and the temperature of walls - 1050 °C, requires a creation of new types of heatproof steels. For the said purpose, highly alloyed materials, such as and Cr35Ni45 alloy, were created [3, 4].

Within several latter decades, many scientists were involved in investigation of degradation of microstructure of exploited high temperature alloys and forecasting the operational life of pipes usually produced of alloys of the classes HK and HP. However, data on the newly created Cr35Ni45 allow are not abundant [5].

Heatproof alloys are widely used in petrochemical industry, namely, in pyrolysis and reforming furnaces where the equipment operates under extreme conditions.

If the said alloys are used at a high temperature and in aggressive media for a long period, a degradation of their mechanical properties takes place; however, it is not usually detected on the mechanical tests, because the degradation process does not progress dramatically and the mechanical properties of the steel conform to the minimum applicable standards set in the norming documents. So, for exploring the causes of crack formation, a considerable attention shall be paid to the mechanical properties and the microstructure [6].

Upon striving to get to know whether the exploitation causes a deterioration of properties of high temperature Ni-Cr steel and an appearance of cracks, the following tests were carried out in course of the research: hardness and microhardness measurement according to Vickers method and investigation of the microstructure.

1. The methodology of the research

In this paper, the object of research is high temperature Ni-Cr alloy. Heatproof alloys replaced the traditional nickel superalloys, their properties are equivalent to those of the latter and they are distinguished for excellent resistance to oxidation and high temperature. At present, GX40NiCrNb 45-35 alloy is up-and-coming, because a traditional material is prone to cracking after a long operation at a higher temperature. The principal applications of this alloy are convection coil pipes and tubes sheets for furnaces. This alloy is considered one of the most important in the oilfield.

A tubes sheet (Figs 1 and 2) is a monolithic product similar to several interconnected I-shaped beams with the following dimensions: the length – 4300 mm, the height – 1300 mm, and the width – 250 mm. The sheets are fixed to the both ends of lateral walls of the convection section.

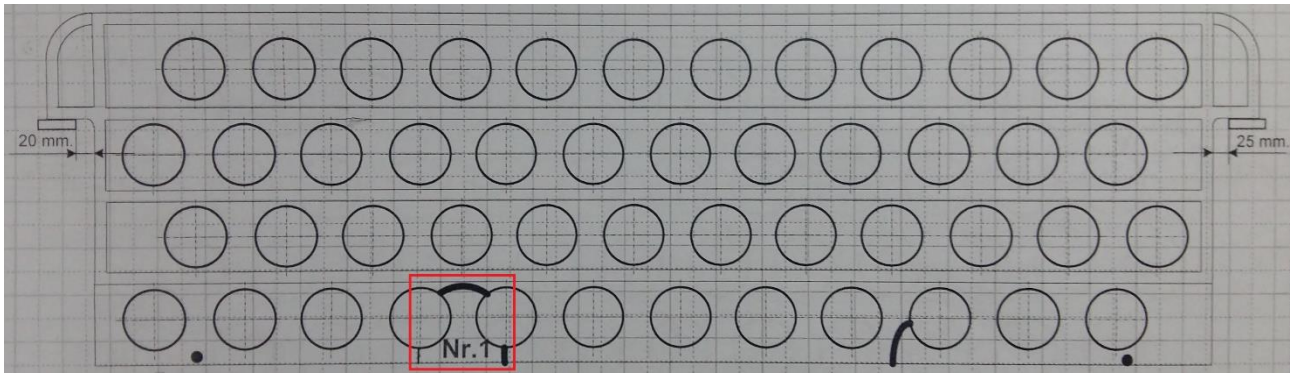

Fig. 1. - The scheme of the tubes sheet of the coil tube in the furnace with cracks No. 1

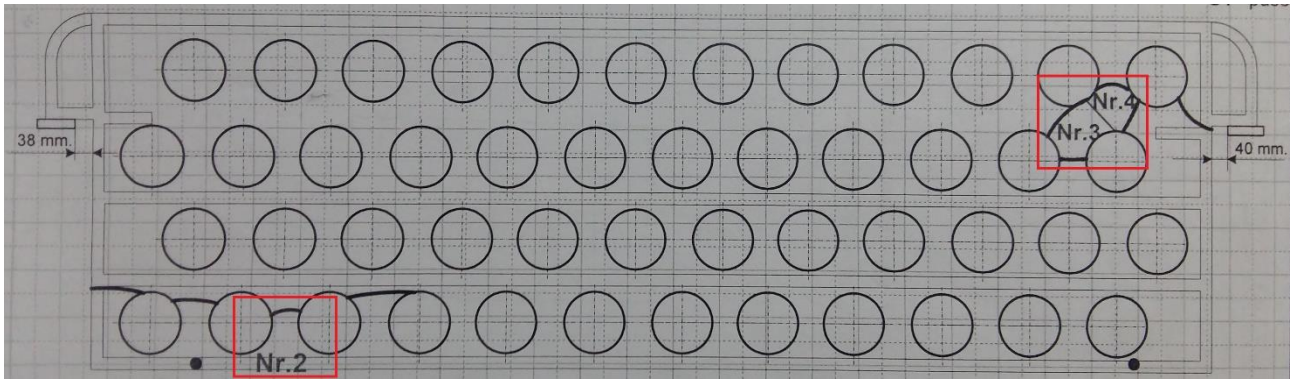

Fig. 2. - The scheme the tubes sheet of the coil tube in the furnace with cracks No. 2, 3, 4

Each the tubes sheet of the coil tube has a number technological holes for inserting pipes of the convection pipework. During repairs, an inspection of the tubes sheet of the coil tube exploited by since 2008 showed that cracks of the tubes sheet of the coil tube appeared between the technological holes.

It is evident that a load exceeding the allowable values or a sudden appearance of loads in the pipes or tubes sheets are hardly probable because of permanent control (monitoring) of the exploitation parameters. Nevertheless, vibrations in the pipe are possible during operation. The performance data enable to establish that the furnace was stopped for the planned repairs only.

Hereinafter the chemical composition of steel GX40NiCrNb45-35 (EN 1.4889) under research (Table 1) and its mechanical properties (Table 2) are provided.

Table 1. The chemical composition of steel GX40NiCrNb45-35 (EN 1.4889), %

Element	C	Si	Mn	P	S	Cr	Ni	Nb	Fe
Min.	0.35	1.50	1.00	-	-	32.50	42.00	1.50	balance
Max.	0.45	2.00	1.50	0.040	0.030	37.50	46.00	2.00	balance

Table 2. The mechanical properties of steel GX40NiCrNb45-35 (EN 1.4889)

R_m – tensile strength	440 MPa
$R_{p0.2}$ – yield strength	240 MPa
A - min. relative elongation on breaking	3 %

Measurements of hardness of the investigated specimens were carried out on polished microsections upon applying versatile automated hardness meter „ZwickRoell ZHμ“ (a measurement error 1 %).

Measurements of individual phases of metal microstructure were carried out upon applying the Vickers method at the load of 10 g (HV0.01) and the holding time of 10 s. Measurements of microhardness of the metal matrix were carried out upon applying the Vickers method at the load of 100 g (HV0.1) and the holding time of 10 s. The average value of metal microhardness was calculated on the base of 5 results of measurements.

In addition, measurements of microhardness were carried out on edges (location of a break) and the central part of the specimens. A load of 2 kg (HV2) and the holding time of 10 s were applied. The average value of hardness on edges of the specimens was calculated on the base of 10 results of measurement and the average value of hardness on the central part - on the base of 5 results of measurements.

During the research, upon striving to establish the number of structural components of the alloy and their dislocation as well as structural alterations having appeared on thermal, thermochemical, mechanical and other processing, the defects of metal (such as slag inserts, pores, cracks and so on) and nonmetal inserts in metal (such as oxides, sulphides, phosphides, nitrides and so on), macro- and microanalysis of specimens under research were carried out.

Specimens for microsections were cut out from the fragment with the best visible metal structure. The plane chosen for microanalysis of the specimens under research was polished with sandpaper of different roughness (from P250 to P2500); for cooling, water was used. For increasing the efficiency of polishing, KEMET polishing suspension (the size of particles - up to 1μm) was used. During the tests of the microstructure of the specimens, aqua regia was chosen for etching (the etching temperature was 20 ºC, and its duration was 5 minutes).

Optical macro- and microscopy tests were carried out by analytics microscope „Nikon MA200“ with „OptiCam“ video camera. The microstructure was tested upon applying objectives wit 5x, 10x, 20x and 50x magnification and an ocular with 10x magnification.

The scanning electron microscopy (SEM) tests, with a parallel analysis of the chemical composition of components upon applying the sectoral and spot x-ray microanalysis method, were carried out by scanning electron microscopy (SEM) device SEM JEOL JSM-7600F with SE detector of secondary electrons. The parameters of electron microscopy were: accelerating voltage 10 kV, distance to the surface of the specimen 11 mm, magnification from 50x 1000x, temperature 22 °C.

2. Results and discussion

For the macro- and microanalysis, the microsections of the tubes sheet made of steel GX40NiCrNb45-35 were prepared of after 10 years of its exploitation. The specimen under research was ground with cooling by water to avoid possible changes of the microstructure and then polished.

While testing the macrostructure of the polished specimen, carbides, nonmetal inserts and various microdefects (such as microcracks, pores and so on) can be found.

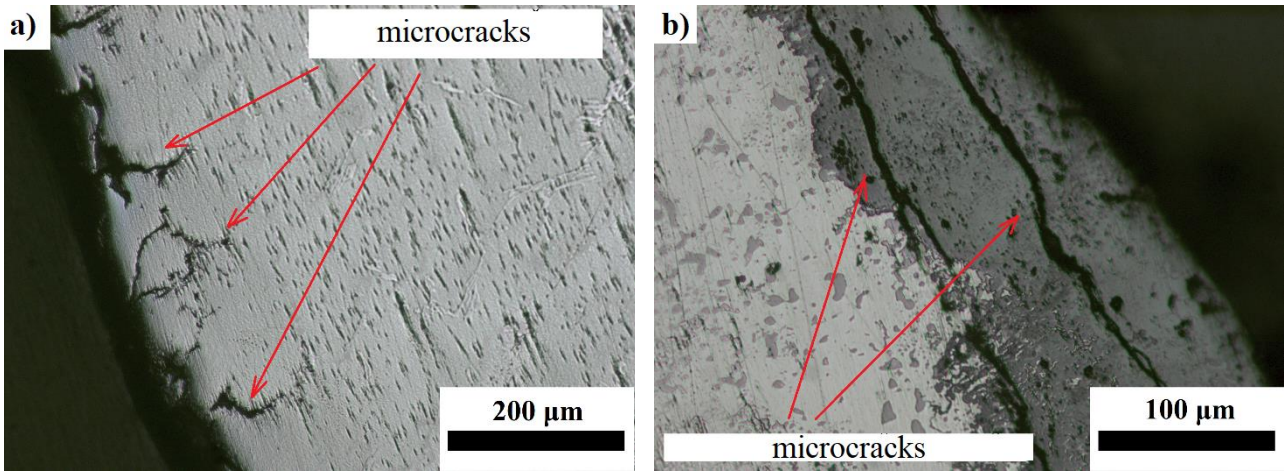

Fig. 3. - Defects in the microstructure of the specimen No. 1

While examining the microsection of the specimen No. 1, microcracks extending from the surface into the depth of the metal (Fig. 3, a) with the length up to 200 μm and microcracks extending along the total length of the microsection in parallel (Fig. 3, b) to the surface were found.

While examining the microsection of the specimen No. 2, nonmetal inserts up to 400 μm were found. They could be sand particles having got in the alloy on casting. In addition, microcracks in parallel to the surface of break with the length about 400 μm were found.

While examining the microsection of the specimen No. 4, nonmetal inserts extending from the surface into the depth of the metal with the length from 100 μm to 400 μm were found.

For highlighting the structure of metal, the polished plane was etched with a special reagent - aqua regia. The composition of individual phases of the material‘s microstructure will be established on scanning electron microscopy SEM) tests.

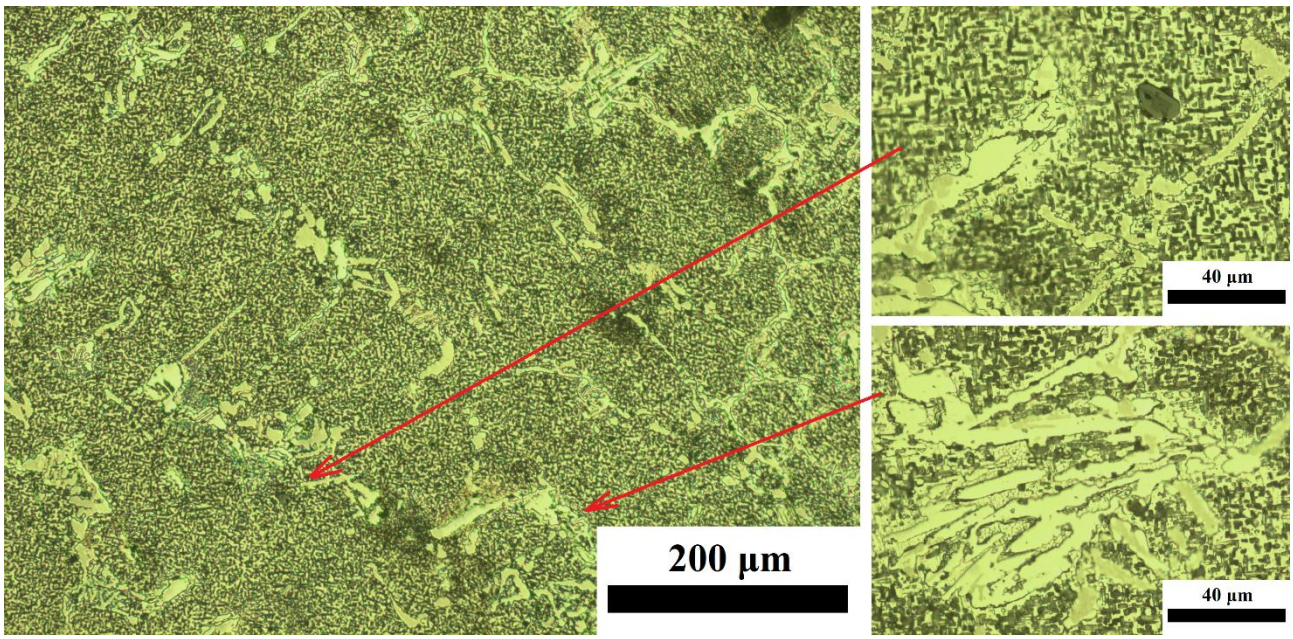

Fig. 4. The microstructure of the specimen No. 1

The results of examining the microstructure of the specimen No. 1 (Fig. 4), the specimen No.2 and the specimen No. 4 through a microscope show the typical microstructure of alloy Fe-Cr-Ni-Nb. Different phases of the microstructure, the metal matrix, various intermetal compounds and various carbides and oxides are clearly visible. The microstructure of these alloys is formed of primary austenite dendrites with various eutectic components, carbides (they can be chromium and niobium carbides) and oxides (they can be chromium oxides) in the interdendrite zones. For more precise identification of the type of steel microstructural components, x-ray microanalysis is required. In course of examination of the microstructure, it was found that microcracks spread from the surface to the depth of metal between dendrites of austenite matrix.

The measurements of microhardness of individual phases of the microstructure of the metal alloy (the phases 1-3 and the phase 5) and the metal matrix (the phase 4) were carried out upon applying micro Vickers method (Fig. 5). The arithmetic values provided in the paper were calculated after a prior rejection of the maximum and the minimum values of 5 results of measurement (Table 3).

Table 3. The results of measurement of microhardness of phases of the specimen's microstructure

Test	1 phase	2 phase	3 phase	4 phase	5 phase
1	1119 HV	272 HV	519 HV	108 HV	1476 HV
2	1106 HV	258 HV	565 HV	112 HV	1403 HV
3	1106 HV	244 HV	561 HV	106 HV	1549 HV
4	1082 HV	356 HV	578 HV	114 HV	1451 HV
5	1250 HV	291 HV	741 HV	107 HV	1428 HV
Average	1102 HV	274 HV	568 HV	109 HV	1452 HV

While analysing the results of the research, it can be observed that microhardness of individual phases of the microstructure differs from microhardness of the metal matrix 2–14 times. Such a difference can be caused by various intermetal compounds, oxides and carbides.

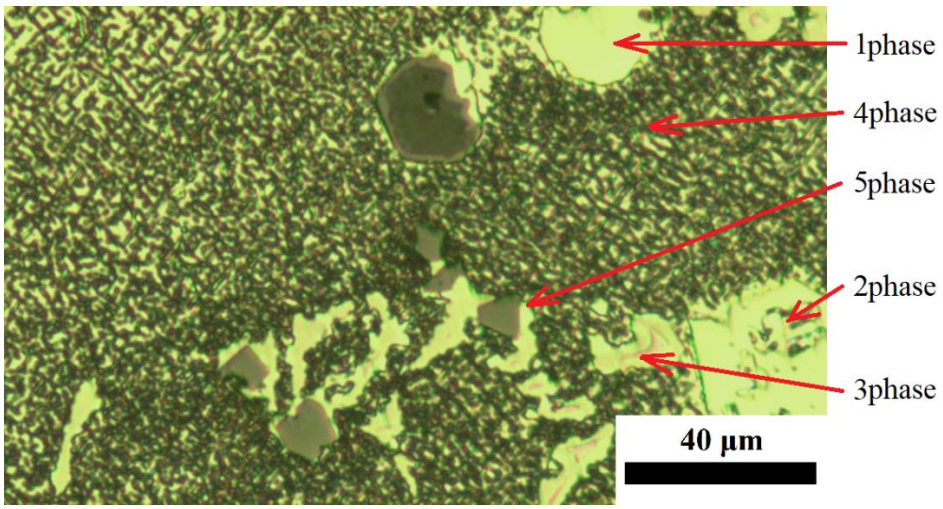

Fig. 5. - The scheme for measuring the microhardness of microstructural phases

Microsections of tubes sheet made of steel GX40NiCrNb45-35 exploited for 10 years were investigated upon applying SEM method; in addition, the chemical composition of the microstructural components was explored upon applying the sectoral and spot x-ray microanalysis method. The scheme of the investigation is presented in Fig. 6. and the results of it – in Table 4.

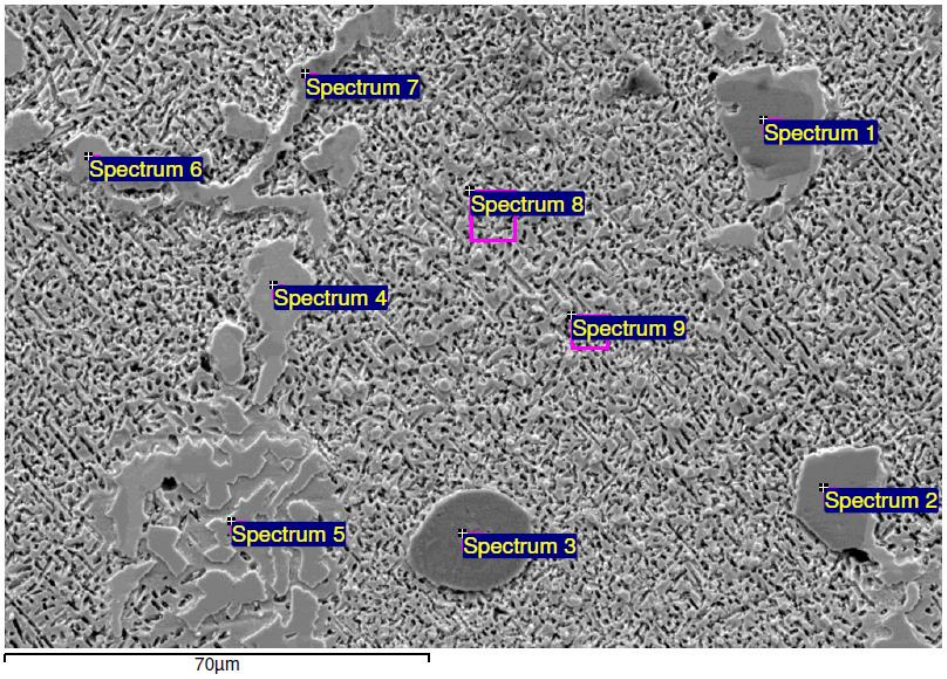

Fig. 6. - The scheme for spot x-ray microanalysis of a specimen made of steel GX40NiCrNb45-35

Table 4. The results of examination of the chemical composition

Zone	C	O	Al	Si	Ti	Cr	Mn	Fe	Ni	Nb
1	–	23,01	2,51	–	2,33	48,22	23,93	–	–	–
2	–	22,83	1,78	–	1,90	49,39	24,10	–	–	–
3	–	26,64	3,08	10,03	2,61	47,04	10,59	–	–	–
4	–	0,27	–	5,59	–	16,14	–	7,01	53,85	17,14
5	4,53	–	–	1,33	–	26,75	0,81	20,49	46,09	–
6	–	1,22	–	4,04	–	11,46	–	–	40,70	42,59
7	9,09	–	–	3,34	–	35,05	–	4,74	37,59	10,20
8	–	2,86	–	1,28	–	13,27	9,41	21,06	52,12	–
9	–	3,27	–	1,43	–	11,23	8,29	21,38	51,27	1,31
Total area spectrum	–	–	–	3,41	–	27,57	1,53	16,59	45,08	5,85

The results of x-ray microanalysis of the specimens under research show that the chemical composition of exploited steel GX40NiCrNb45-35 generally meets the provisions of the standard. Some higher Nb and Si contents and lower Cr content may be caused by the circumstance that the x-ray microanalysis was made on an area that was less, as compared to areas usually used by chemical analyzers or metals. While accomplishing microstructural tests of microsections, 6 microstructural phases were observed. The results of x-ray microanalysis of individual microstructural phases show that the phase 1 (the point 5) can be identified as Cr carbides in Ni-Fe matrix; the phase 2 – as NiNbCr intermetal compound; the phase 3 (the point 6) – as NbNiCr intermetal compound; the phase 4 (the points 8 and 9) – as austenite Fe-Ni matrix enriched with Cr, Nb, Si, and Mn; the phase 5 - as CrNb carbides in Ni-Fe matrix and the phase 6 (the points 1-3) – as CrMn and CrMnSi oxides. The results of x-ray microanalysis correlate with the results of microhardness tests of individual phases.

Conclusions

1. In course of the research on the macrostructure of exploited convection furnace coil pipes and tubes sheets, large nonmetal inserts and microcracks (parallel and perpendicular to the surface under research) were found. The microcracks spread from the surface into the depth of metal between dendrites of austenite matrix.
2. The results of the microstructural tests show that the microstructure of alloy Fe-Cr-Ni-Nb is formed of primary Fe-Ni austenite dendrites with various eutectic components, NiNbCr and NbNiCr intermetallic compounds, carbides (they can be chromium and niobium carbides) and oxides (they can be CrMn and CrMnSi oxides) in the interdendrite zones. The microhardness of individual phases of the microstructure differs from microhardness of the metal matrix 2–14 times.
3. In course of the research it was found that metal hardness of the exploited tubes sheet is similar on the surface and the central part of it and conforms to hardness of the non-exploited material.
4. The tests of the mechanical properties of the tubes sheet show that plasticity and impact tensility of alloy Fe-Cr-Ni-Nb decrease in course of exploitation of the equipment.
5. Upon summarizing the results of the research, it may be stated that an appearance of cracks in metal of the tubes sheet can be caused by deterioration of mechanical of the exploited metal, the influence of long-lasting tension and high temperature as well as changes of loads on startup/shutdown of the equipment.

References

[1] Sustaita-Torresa, I.A., Haro-Rodríguez, S., Guerrero-Mata, M.P., De la Garza, M., Valdés, E., Deschaux-Beaume, F., Colásb, R. Aging of a cast 35Cr–45Ni heat resistant alloy //Materials Chemistry and Physics, 133, 2012. – P.1018 – 1023.
[2] Piekarski, B., Kubicki, J. Creep-resistant austenitic cast steel //Archives of foundry engineering, Volume 8, Issue 2/2008. - P. 115 - 120.
[3] Zhao, Y., Gong, J., Yong, J., Wang, X., Shen, L., Li, Q. Creep behaviours of Cr25Ni35Nb and Cr35Ni45Nb alloys predicted by modified theta method // Materials Science & Engineering A, 649, 2016. – P. 1 – 8.
[4] Cheng C., Li H., Zhao, J., Min, X. Microstructural analysis of Cr35Ni45Nb heat-resistant steel after a five-year service in pyrolysis furnace. Engineering Failure Analysis, 79 (2017). – P. 625 – 633.
[8] Song, R., Wu, S. Microstructure evolution and residual life assessment of service exposed Cr35Ni45 radiant tube alloy. Engineering Failure Analysis, 88, 2018. – P. 63–72.
[9] Gulshan, F., Ahsan, Q., Haseeb, A.S.M.A, Haque, E. Failure Analysis of Superheater Tube Supports of the Primary Reformer in a Fertilizer Factory //Journal of Failure Analysis and Prevention, Volume 5 (3). - P.67 - 72.

Information of the authors

Lukašius Denis, master, assistant of the department ”Mechanical Engineering and Materials Science” of Vilnius Gediminas technical university
E-mail: denis.lukasius@vgtu.lt

Buzaitis Kęstutis, bachelor, engineer of the department ”Mechanical Engineering and Materials Science” of Vilnius Gediminas technical university
E-mail: kestutis.buzaitis@stud.vilniustech.lt

Černašėjus Olegas, Phd, associate professor of the department “Mechanical Engineering and Materials Science” of Vilnius Gediminas technical university
E-mail: olegas.cernasejus@vgtu.lt

Žlioba Karolis, bachelor, assistant of the department of Mechanical Engineering and Materials Science of Vilnius Gediminas technical university
E-mail: karolis.zlioba@vilniustech.lt.